Journal of Advanced Ceramics
2022, **11**(5): 665–701
https://doi.org/10.1007/s40145-022-0567-5
ISSN 2226-4108
CN 10-1154/TQ

Review

Advances in 3D printing of magnetic materials: Fabrication, properties, and their applications

Xiangxia WEI[a], Ming-Liang JIN[a], Haiqiang YANG[a], Xiao-Xiong WANG[b], Yun-Ze LONG[b], Zhangwei CHEN[c,*]

[a]*Institute for Future*, *School of Automation*, *Shandong Key Laboratory of Industrial Control Technology*, *Qingdao University*, *Qingdao 266071*, *China*
[b]*Collaborative Innovation Center for Nanomaterials & Devices*, *College of Physics*, *Qingdao University*, *Qingdao 266071*, *China*
[c]*Additive Manufacturing Institute*, *College of Mechatronics and Control Engineering*, *Shenzhen University*, *Shenzhen 518060*, *China*

Received: August 4, 2021; Revised: October 25, 2021; Accepted: January 8, 2022

Abstract: Magnetic materials are of increasing importance for many essential applications due to their unique magnetic properties. However, due to the limited fabrication ability, magnetic materials are restricted by simple geometric shapes. Three-dimensional (3D) printing is a highly versatile technique that can be utilized for constructing magnetic materials. The shape flexibility of magnets unleashes opportunities for magnetic composites with reducing post-manufacturing costs, motivating the review on 3D printing of magnetic materials. This paper focuses on recent achievements of magnetic materials using 3D printing technologies, followed by the characterization of their magnetic properties, which are further enhanced by modification. Interestingly, the corresponding properties depend on the intrinsic nature of starting materials, 3D printing processing parameters, and the optimized structural design. More emphasis is placed on the functional applications of 3D-printed magnetic materials in different fields. Lastly, the current challenges and future opportunities are also addressed.

Keywords: three-dimensional (3D) printing; hard magnets; soft magnets; magnetic properties; applications

1 Introduction

Magnetic materials are typically referred to objects that could produce their own magnetic field, and the overall magnetic behaviors are particularly depending on the orbit and spin motions of electrons. From the aspect of behavior under magnetic field, magnetic materials can be divided into several categories, such as ferromagnets, ferrimagnets, paramagnets, and diamagnets. As essential components in many electrical devices [1–3], including motors, generators, transformers, magnetic recording, etc., it is incontrovertible that the widespread applications of magnetic materials strongly lie in the availability to manufacture structures with required geometries and architectures. Some traditional manufacturing techniques, such as casting [4–6], injection molding [7–9], and compaction [10–12] have been widely used. However, it is limited to very simple shapes with the post machining processes to achieve the user-defined geometries, and

* Corresponding author.
E-mail: chen@szu.edu.cn

Nomenclature

2PP	Two-photon polymerization	D_m	Critical single domain limit	PBAM	Powder bed additive manufacturing
3D	Three-dimensional	EBM	Electron beam melting	PCL	Polycaprolactone
ABS	Acrylonitrile butadiene styrene	EEA	Ethylene ethyl acrylate	PDMS	Polydimethylsiloxane
AM	Additive manufacturing	EFF	Extrusion free forming	PLA	Polylactic acid
BAAM	Big area additive manufacturing	FDM	Fused deposition modeling	PVA	Polyvinyl alcohol
$(BH)_{max}$	Maximum energy product	FFF	Fused filament fabrication	RC	Robocasting
BJ	Binder jetting	H_c	Coercive field or coercivity	SL	Stereolithography
CAD	Computer-aided design	HGMS	High gradient magnetic separation	SLM	Selective laser melting
CLIP	Continuous liquid interface production	LENS	Laser engineered net shaping	SLS	Selective laser sintering
DEG	Diethylene glycol	M_r	Remanent magnetization	T_C	Curie temperature
DIW	Direct ink writing	M_s	Saturation magnetization		
DLP	Digital light processing	PA	Polyamide		

sometimes expensive molds were required. At the same time, residues are generated during most manufacturing processes, and the volume of residues rapidly scales up as a result of the large market of magnetic materials [13]. To allow the production of magnetic materials with net-shaped customized shapes in accordance to some specific applications, an increasing number of studies have been devoted to developing new technologies.

As an emerging advanced technology, three-dimensional (3D) printing, also known as additive manufacturing (AM), has attracted growing attention due to its unique capability for the freeform construction with complex 3D features and diversity of the compatible materials, including polymers [14–18], metals [19–21], ceramics [22–29], composites [30–36], etc. Moreover, 3D printing is capable of implementing the desired design with unprecedented complexity and functionality. Unlike traditional techniques that require dies, molds, or any machining operations, 3D printing offers tremendous cost and time saving, especially for ceramics. At the same time, 3D printing has the ability of shape control and multi-material printing, thus constructing structures that are previously unachievable. Therefore, this technology is increasingly used in various applications ranging from electronics [34,37–41], robotics [42–44], and biomedical engineering [45–49], to energy and environmental applications [39,40,50–55].

With the development of 3D printing technology, it offers huge opportunities for the manufacturing of magnetic materials with shape complexity and excellent properties while reducing waste excess materials. The problem of materials waste is particularly challenging for permanent magnets since they are commonly composed of rare earth elements which are defined as critical materials. Notably, a few impressive results have been achieved [36,56–71]. However, 3D printing of magnetic materials is still challenging: (1) Limited types of printable materials. Some materials with excellent magnetic properties could not be printed, and the most permanent magnets are bonded magnets. (2) Low printing resolution and speed. (3) Poor magnetic properties due to the fact that their elevated complexity from the materials. Therefore, to unleash the possibility of 3D printing of magnetic materials, the materials and processes need to be discussed. Although there are several review articles that partially mention 3D printing of magnetic materials particularly permanent magnets [72–76], to the best of our knowledge, few review has given a comprehensive introduction on 3D-printed magnetic materials with high performance and their magnetically functional applications.

Based on the above, in this review, the recent advances centering on 3D printing of magnetic materials are summarized and reviewed. In Section 2, certain basic knowledge of magnetic properties is briefly introduced, and 3D printing strategies for fabrication of magnetic materials are highlighted in Section 3. In Section 4, 3D-printed magnetic materials are divided into three categories, such as permanent magnets, soft magnetic materials, and magnetic composites, and their corresponding 3D printing approaches and magnetic properties are summarized and analyzed. In Section 5, the applications of 3D-printed magnetic materials are exhaustively discussed, such as in soft robotics, transformers, drug delivery, microwave absorption, magnetic separation, and magnetic levitation as illustrated

in Fig. 1. Lastly, the current research profiles, challenges, and perspectives of 3D-printed magnetic materials are addressed.

2 Overview of magnetic materials

In this section, the understanding of magnetic properties of materials and 3D printing techniques will be briefly introduced, since it is essential for the fabrication of tailored structures with specific magnetic properties by selecting materials for the exploration of the potential applications.

In the viewpoint of behavior under the external magnetic field, there are several types of magnetic materials, such as ferromagnetics, ferrimagnetics, antiferromagnetics, paramagnetics, and diamagnetics as depicted in Fig. 2. In the case of ferromagnetic materials, there are a few unpaired electrons in materials, and magnetic domains tend to be parallel to each other with

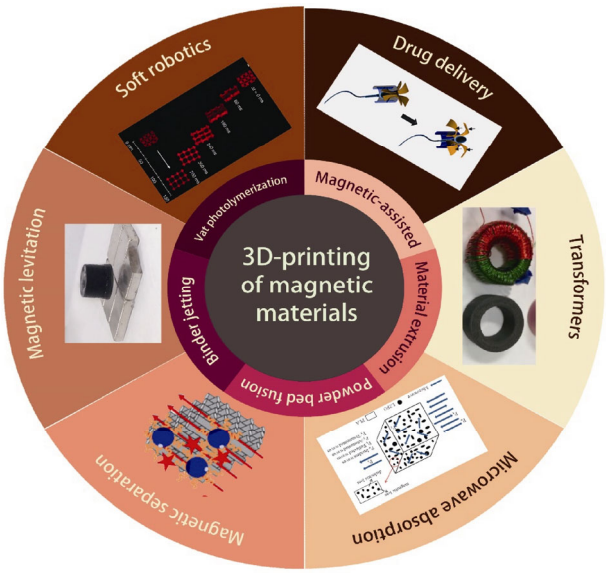

Fig. 1 Applications of 3D-printed magnetic materials. Representative applications are soft robotics (reproduced with permission from Ref. [36], © Macmillan Publishers Ltd., part of Springer Nature 2018), drug delivery (reproduced with permission from Ref. [77], © American Chemical Society 2017), transformers (reproduced with permission from Ref. [78], © Elsevier B.V. 2017), microwave absorption (reproduced with permission from Ref. [79], © Springer Science Business Media, LLC, part of Springer Nature, 2018), magnetic separation (reproduced with permission from Ref. [50], © American Chemical Society 2017), and magnetic levitation (reproduced with permission from Ref. [80], © The Royal Society of Chemistry 2017).

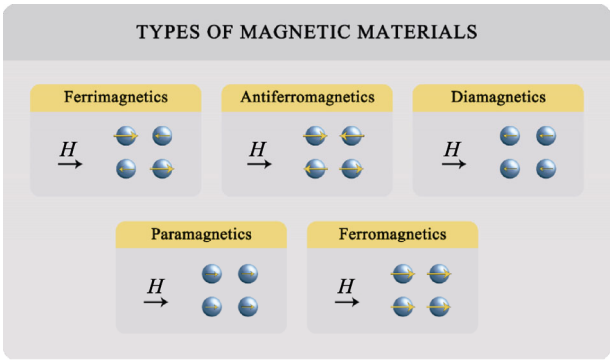

Fig. 2 Schematic illustration of types of magnetic materials.

the presence of applied magnetic field. Therefore, significant magnetism can be produced and retained even after removal of the external field. For paramagnetic materials, there are some unpaired electrons and materials that can be partially magnetized when subjected in an external magnetic field. However, the magnetic moment quickly drops to zero when the external field is removed due to the non-interaction of individual magnetic moment. Moreover, a diamagnetic material, e.g., superconducting magnets, can be repelled by an external magnetic field.

To date, ferromagnetic/ferrimagnetic materials are usually utilized to fabricate functional magnetic systems by 3D printing approaches. On the basis of magnetic property of coercivity, ferromagnetic and ferrimagnetic materials can be generally divided into hard magnets with high coercivity that are difficult to be demagnetized, and soft magnets with relatively low coercivity that can be easily demagnetized. In the case of hard magnets (also called permanent magnets), significant magnetic hysteresis starting from non-magnetized state is exhibited as depicted in Fig. 3(a) [81]. Even when the external field is reduced to zero, the materials are capable of retaining a high remanent magnetization (M_r). One needs to apply a field in the opposite direction to bring the magnetization to zero. The applied field is called the coercive field or coercivity H_c. Generally, H_c increases with an increase of grains, but it starts to decrease for a further increase of grains when exceeding the critical single domain limit (D_m). The critical size of a single-domain particle can be estimated by Eq. (1) [82]:

$$D_m = 9\sigma_w / \left(2\pi M_s^2\right) \quad (1)$$

where $\sigma_w = \left(2k_B T_C |K_1| / a\right)^{1/2}$ is the wall density energy, M_s is the saturation magnetization, $|K_1|$ is a magnetocrystalline anisotropy constant, k_B is the Boltzmann constant, T_C is the Curie temperature, and a

is a lattice constant.

The main goal in permanent magnets is the maximization of hysteresis loop area by improving M_r, H_c, and the resultant maximum energy product $(BH)_{max}$, which quantifies the magnetostatic energy the material can store therefore represents how strong the magnet is [83]. $(BH)_{max}$ is related to the $B(H)$ loop, which is deduced from the $M(H)$ loop via the defining Eq. (2):

$$B = \mu_0(H + M) \tag{2}$$

where B is the magnetic induction (T), H is the magnetic field (A/m), M is the magnetization (A/m), and $\mu_0 = 4\pi \times 10^{-7}$ H/m is the permeability of vacuum. The development of $(BH)_{max}$ of hard magnetic materials is illustrated in Fig. 3(b) [84], and the enhancement of energy product has been achieved by microstructure engineering [84] and exchange spring coupling between soft/hard magnetic phases [85]. The main hard or semi-hard magnetic materials are $R_2Fe_{14}B$ intermetallics (typically with R = Nd, Sm, Y, Pr, Dy, and Ce) and Sr/Ba ferrites.

In contract, soft magnetic materials highly rely on the applied magnetic field, which can be magnetized and demagnetized easily with high M_s and low coercivity. They tend to return to a state of low residual magnetization when the magnetic field is removed. Therefore, soft magnetic materials are widely used as cores of transformers, inductor, and motors. Other fundamental materials properties such as permeability and losses can be explored elsewhere [86]. The main soft magnets include (Ni, Zn) ferrite, (Mn, Zn) ferrite, FeSi, FeNi, etc. [87].

For paramagnetic and diamagnetic materials, the magnetization is induced that is linear with an applied magnetic field as described in Eq. (3):

$$M = \chi H \tag{3}$$

where χ is the magnetic susceptibility: $\chi > 0$ for paramagnetic and $\chi < 0$ for diamagnetic materials. This means that the direction of M is parallel to H for paramagnetic materials and antiparallel to H for diamagnetic materials [88]. Combining Eqs. (2) and (3), Eq. (4) is given:

$$B = \mu H \tag{4}$$

where $\mu = \mu_0(1 + \chi)$ is the permeability of the material.

It is well-recognized that magnetic materials are key components in electronics, data processing, and the automotive industry. Instead of traditional manufacturing (e.g., cutting, machining, etc.) generating waste material, the state-of-the-art 3D printing technology is well-suited to fabricate magnetic materials which usually involve the critical rare earth elements [89]. In Section 3, the basic principles of 3D printing technique will be introduced.

3 3D printing technologies for the fabrication of magnetic materials

3D printing, a layer-by-layer deposition technology, enables the realization of 3D architectures directly from digital design with printers under computer numerical control [90]. Unlike traditional manufacturing methods that require dies, expensive molds, or any machining operations, 3D printing can convert computer-aided design (CAD) models into 3D structures on demand [91,92]. According to different printing principles, there are several technologies that have been developed to meet the needs of different materials. Here, basic 3D printing techniques are described to provide a fundamental understanding for the fabrication of magnetic materials,

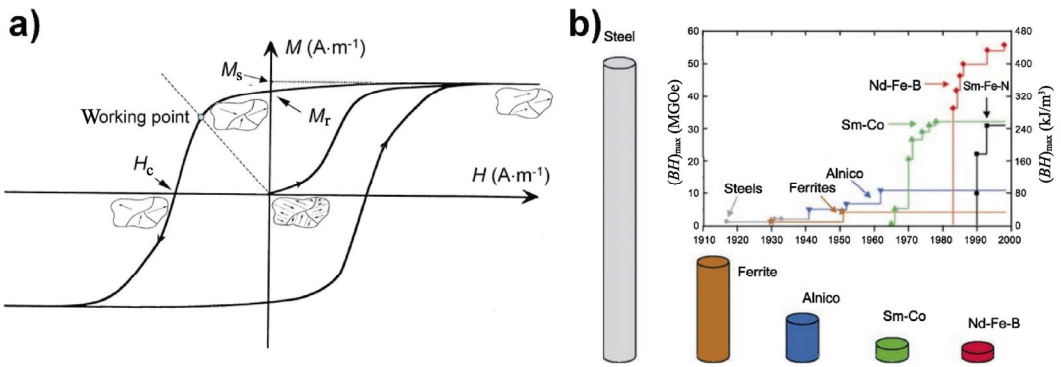

Fig. 3 (a) An hysteresis loop for a hard magnetic material. Reproduced with permission from Ref. [81], © IEEE 2011. (b) Development in the $(BH)_{max}$ of hard magnetic materials in the 20th century. Reproduced with permission from Ref. [84], © IOP Publishing Ltd 2000.

and the performances of 3D-printed features are then given and discussed. For comparison, these fabrication methods, as well as their advantages and weaknesses, are summarized.

3. 1 Vat photopolymerization

Vat photopolymerization is an AM process that constructs objects with selectively cured photopolymer using specific light (e.g., UV radiation) via photopolymerization. The first developed method was stereolithography (SL) in the early 1980s as shown in Fig. 4(a) [93]. In SL, a liquid resin is selectively photopolymerized by UV light to form a thin layer of patterned solid during printing. Once a layer is finished, the substrate moves by one-layer thickness, and a new layer of liquid resin is introduced into the print regions followed by the sequential polymerization. The process is repeated in a layer-by-layer fashion until the designed structure is completed [94]. To meet the requirement of high resolution and speed, various techniques have been developed, including digital light processing (DLP) [95,96], continuous liquid interface production (CLIP) [97], and two-photon polymerization (2PP) [98–100]. Although they are all based on the basic concept of SL, DLP and CLIP enable the solidification of an entire layer by using the digital micro-mirror device [96] or liquid crystal on silicon chip [101] as the dynamic masks to project a mask pattern onto the resin reservoir. Therefore, the printing speed of DLP and CLIP is much faster than that of SL. To date, 2PP provides the highest printing resolution of ~100 nm.

Based on this, many researchers have printed magnetic materials using these 3D printing techniques [56,102–104]. Despite its promising potential, vat photopolymerization-based 3D printing is still challenging due to the presence of magnetic particles in the resin matrix: (1) High solid loading of magnetic particles increases the viscosity of the liquid resin, thereby reducing the printability of

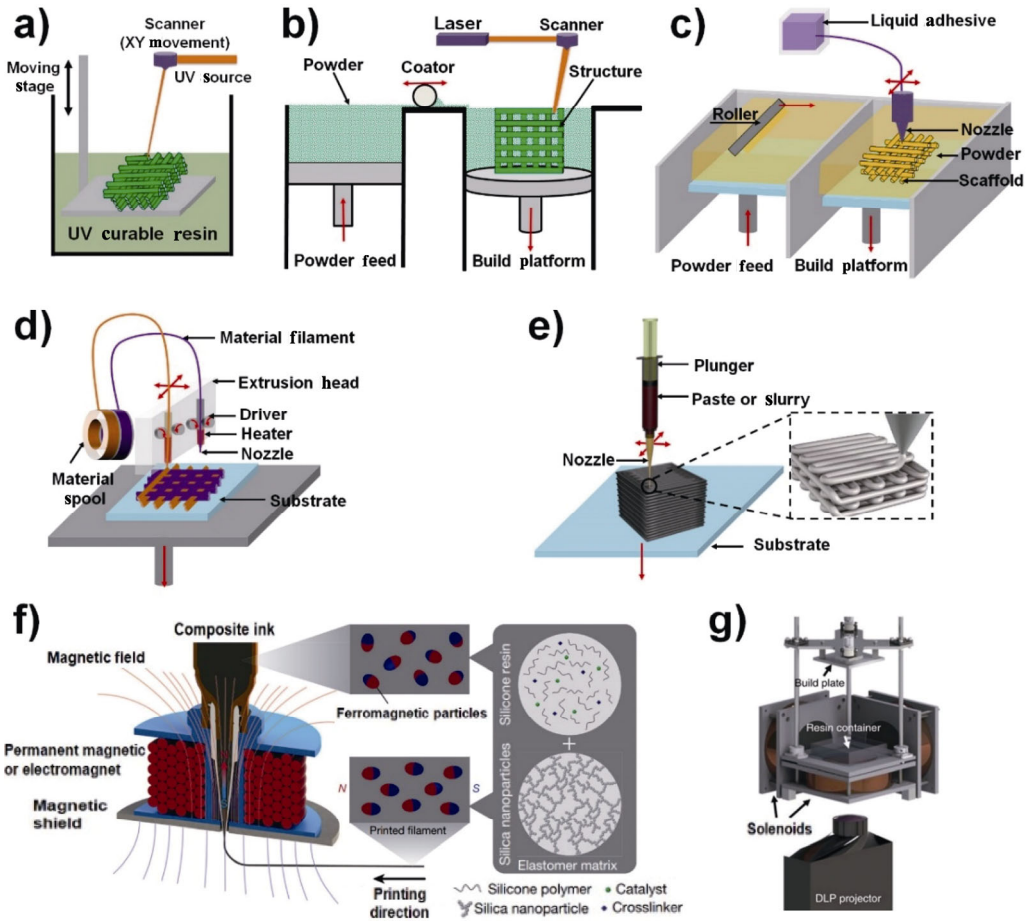

Fig. 4 Schematic diagrams of 3D printing technologies: (a) SL technique, (b) SLS, (c) BJ, (d) FDM, and (e) DIW or EFF. (f) Magnetic field assisted DIW. Reproduced with permission from Ref. [36], © Macmillan Publishers Ltd., part of Springer Nature 2018. (g) DLP with a magnetic field. Reproduced with permission from Ref. [65], © The Author(s) 2015.

materials and slowing down the fabrication speed. (2) Large particles are prone to precipitation and sedimentation under gravity force, which compromises the reliability of 3D printing. (3) Magnetic powders with dark color would induce strong light scattering and light adsorption, resulting in a partial polymerization.

3. 2 Powder bed fusion

Powder bed fusion is an AM process that uses a laser as power source or polymeric binder to bond powdered materials together for the creation of a solid structure. Several commonly techniques are used to investigate to print magnetic materials, including selective laser sintering (SLS) [105], selective laser melting (SLM) [106], electron beam melting (EBM), laser engineered net shaping (LENS) [107], and binder jetting (BJ) [64] according to the phase state of powders when binding. As depicted in Fig. 4(b), SLS is a powder bed printing technique by the selectively locally heating polymer particles and fusing together by a powerful laser beam (e.g., CO_2, Nd:YAG laser) [108,109]. When one layer has been printed, successive layer is spread across the bed with the platform down by one-layer thickness, and the laser beam repeats locally heating and fusing powders together based on the predefined geometries. The non-fused powders serve as a support material during the printing process. After the final object has been completed and removed from the printing bed, the loose powders can be recycled. Within the SLS process, the properties of 3D objects are strongly determined by material and processing parameters, including particle size and distribution, laser energy, spot size, hatch distance, and layer thickness [108]. In general, powders used in SLS should exhibit good flowability with a spherical morphology to increase the quality of printed parts [110]. Moreover, the minimum feature size achieved by SLS is approximately 100 μm.

Similar to SLS, SLM is a well-known AM technology to produce near full dense metallic objects without the need for post-processing, including Fe-based systems [111–114]. In general, microstructures and magnetic properties of components processed by SLM are mainly influenced by processing parameters (e.g., laser power, scanning velocity, layer thickness, etc.) and powder characteristics [115]. Nevertheless, SLM is usually accompanied by residual stresses, arising from the high thermal gradients in the material when the powders are irradiated with high energy intensities. Also, the vaporization of elements is a severe impediment especially for NdFeB magnets with complexity in the ternary phase diagram [116]. In some cases, EBM is another powder bed additive manufacturing (PBAM) method with certain specific features in context of shaping magnetic materials. EBM is carried out in high vacuum and at high temperatures, which are desirable for metal materials with easily oxidation. In addition, LENS is developed for near-net shaping metal parts which utilizes a high-powered laser to melt powders that is injected toward the focal point of the beam [117]. During printing, the laser and powder feed system remain stationary, and the multi-axis building stage is translated along the scan direction to create geometries following a CAD model.

3. 3 Binder jetting

In contrast to high-power laser-based technology, BJ is also a representative 3D printing method. This technique is based on distributing a liquid binding adhesive to bond loose powders together as illustrated in Fig. 4(c). In an alternative to depositing the material itself, binder solutions can be jetted onto powder beds to locally fuse particles in a method akin to SLS printing. This method has been employed to build magnetic materials with geometric complexity, in particular, the ferrites. The fabrication speed of BJ is recently elevated; however, surface quality is usually very poor resulting from the spreading of liquid into powders [118]. Another limitation of this method is the production of sufficiently dense parts resulting in unsatisfactory magnetic properties, which limits the practical applications. Nevertheless, this porous 3D-printed structures are well suited for an alloy infiltration process to increase the density and magnetic performance of the printed magnets.

3. 4 Material extrusion

Material extrusion is an AM process in which materials are extruded through a nozzle to form a continuous filament with the sequential deposition of multiple layers to build the entity. The first emerged filament printing method was fused deposition modeling (FDM), also known as fused filament fabrication (FFF), schematically illustrated in Fig. 4(d). In FDM, thermoplastic filament as building material is fed into a movable extrusion head, which heats the material into a semi-molten state by a temperature-controlled heater, and subsequently the molten material is deposited and solidified as they cool down below the glass transition

temperature. Some typical polymer matrix can be patterned by this approach, including polylactic acid (PLA), acrylonitrile butadiene styrene (ABS), and ethylene ethyl acrylate (EEA) [119]. By mixing soft or hard magnetic particles into the thermoplastic matrix, FDM can be used to print polymer-bonded magnets, whereas the magnetic properties are mainly affected by the filler orientation and fraction [120]. It is believed that the filling ratios of magnetic parts more than 65 vol% would be necessary [121].

As an alternative to FDM, direct ink writing (DIW), or known as robocasting (RC), extrusion freeforming (EFF), enables to print viscoelastic inks under ambient conditions as shown in Fig. 4(e). Compared with FDM printing, DIW utilizes the air pressure, a piston, or a screw to extrude the printable inks inside the cylinder flowing through nozzles. Thus, the development of printable fluid is crucial to the success of DIW, which requires proper rheological properties that can be extruded through fine nozzles to build up complex 3D architectures. Generally, inks must be tailored to satisfy two important criteria for the continuous printing [122–126]. First, viscoelastic properties are required to allow them to flow through nozzles and then solidify for the shape retention. Second, inks must have a high solid loading to counteract the serious shrinkage during drying. Generally, the inks should exhibit a highly shear thinning flow behavior, approximated by the Herschel–Bulkley model in Eq. (5) [127]:

$$\tau = \tau_{\mathrm{y}} + K\gamma^{n} \tag{5}$$

where τ (Pa) is the shear stress, τ_{y} (Pa) is the yield stress, K (Pa·s^{n}) is a model factor, γ (s^{-1}) is the shear rate, and n is the flow index. When $n < 1$, the fluid shows a shear thinning behavior. That is to say, the apparent viscosity of inks linearly decreases with shear stress in a logarithmic scale.

Considering a laminar and steady flow inside the cylinder and nozzle, the critical condition for printing can be estimated by Eq. (6) [128]:

$$\tau = \left(\frac{\Delta P}{2L}\right) r \tag{6}$$

where ΔP (Pa) is the pressure applied at the nozzle, r (m) is the radius of the nozzle, and L (m) is the length of the nozzle. Similarly, the viscosity (η) of the fluid can be written as Eq. (7):

$$\eta = \frac{\tau}{\gamma} \tag{7}$$

Now, combining Eqs. (6) and (7), the shear rate in the cylinder wall is shown in Eq. (8):

$$\gamma = \left(\frac{\Delta P}{2\eta L}\right) r \tag{8}$$

As inks flow through the nozzle, the maximum shear rate at the nozzle walls can be calculated by Eq. (9) [129–131]:

$$\gamma = \frac{4Q_{\mathrm{v}}}{\pi r^{3}} = \frac{4V\pi r^{2}}{\pi r^{3}} = \frac{4V}{r} \tag{9}$$

where Q_{v} (m^3/s) is the volumetric flow rate, and V (m/s) is the printing speed. Moreover, during the printing process, the ink with particles dispersing in the liquid is extruded at a specific velocity which can be rheologically characterized using the Benbow–Bridgwater equation [132,133]. Although DIW is one of the most common strategies to print diverse materials, the resolution of printed parts is directly limited by the nozzle size and the constant movement of extruder.

3. 5 Magnetic-assisted 3D printing

Considering particle alignment and composition control, some researches utilize magnetic field to assist printing and develop new 3D printing processes. Interestingly, Kokkinis *et al.* [134] demonstrated a magnetically assisted 3D printing method, where anisotropic structures with particle orientation control were built during a DIW process using a rotating low-cost neodymium magnet. The local composition control was implemented by multimaterial dispensers and a two-component mixing unit. In this process, magnetic platelet loading fraction and orientation can be manipulated and controlled in a layer-by-layer way. Similarly, Kim *et al.* [36] proposed a magnetic-assisted DIW printing method to print materials with programmed ferromagnetic domains. This approach is based on printable inks containing magnetizable NdFeB microparticles embedded in a silicone rubber matrix. During printing, an external magnetic field is applied via a permanent magnet around the printing nozzle, which makes NdFeB particles reorient along the field direction as shown in Fig. 4(f). Aligned anisotropic structures were obtained by applying an external magnetic field, indicating great potential in addressing rare earth elements criticality [135].

Besides, magnetic-assisted SL-related 3D printing processes have also been introduced to print magnetic materials. By applying magnetic fields during DLP printing, Martin *et al.* [65] developed a 3D printing

method to produce bioinspired reinforced materials, which controls the orientation of alumina platelets decorated with magnetite nanoparticles (Fig. 4(g)). The magnetic field was applied via electromagnetic solenoids followed with digital mask image polymerization of liquid resin. This technology produced reinforcement architectures with increased stiffness, strength, and hardness properties [136,137]. Lu *et al.* [102] also proposed a magnetic field-assisted projection SL method to control local dispersion of magnetic particles in photopolymer matrix. A high concentration of Fe nanoparticles embedded in liquid polymer was prepared. With the assistance of magnetic field, magnetic particles were induced to specific locations. After that, a digital mask image was used to cure photopolymers with desired orientation and patterns, hence allowing the development of material intelligence by patterning particles in the polymer matrix. In their continuing work, the influences of microscopic distribution parameters on the properties of the 3D-printed composites were characterized [138]. On this basis, the magnetic field assisted projection stereolithgraphy method has been used to fabricate multimaterial soft robot with untethered magnetic actuation, capable of different locomotion functions [139]. More interestingly, the magnetically anisotropic property of the 3D-printed structures could be controlled with the assistance of magnetic field during the 3D printing process [140]. Therefore, such 3D printing methods open new routes for fabricating various 3D smart materials with anisotropic and programmable properties.

Inkjet printing-based AM process can enable the control of particle orientation in each deposited droplet by a suitable external magnetic field. In this case, Song *et al.* [141] reported an inkjet printing technique with magnetic alignment capability. Unlike conventional methodologies, magnetic particles in the ink can be aligned by the application of magnetic field, which promotes the creation of parts with an increase in high frequency permeability and a decrease in hysteresis losses in the alignment-induced axis direction.

3. 6 Summary

Diverse 3D printing techniques have been utilized to pattern the magnetic materials. Vat photopolymerization technologies can selectively solidify the material by dispersing magnetic materials in photosensitive resin. In contrast, material extrusion utilizes the printhead or nozzle to deliver the material to the designed position. These approaches are convenient to change the print material by easily replacing nozzles, which is difficult or even impossible for vat photopolymerization and powder bed fusion technologies. Moreover, for material extrusion, the choice of printable materials is wide as long as they possess suitable rheological properties, thereby enhancing the multi-material printing ability. Nevertheless, vat photopolymerization techniques have advantages in print resolution and build speed. A comprehensive comparison of these 3D printing technologies is listed in Table 1. It is worthwhile to mention that there are no absolute pros and cons of these 3D printing methods, and their performance is heavily dependent on the actual requirements.

4 3D-printed magnetic materials

3D printing has triggered hot research topics related to the fabrication of magnetic materials. In this work, we focus on three kinds of magnetic materials, including hard magnets, soft magnetic materials, and magnetic composites. The relationship among printing parameters, microstructures, and performance is highlighted.

4. 1 Hard magnetic materials

4.1.1 NdFeB permanent magnets

To date, bonded magnets have received accelerated attention in industrial applications due to their advantages such as excellent magnetic properties, shape flexibility, low cost, and superior mechanical properties [154,155]. Instead of conventional compression and injection molding techniques, 3D printing techniques are widely employed to fabricate magnets as summarized in Table 2. For example, BJ has been utilized to print near-net-shape isotropic NdFeB-bonded magnets using ~70 μm sized particles as staring material [64]. Upon completion, the printed green part was cured at temperatures between 100 and 150 ℃. Finally, the density of magnet reached 3.47 g/cm^3 after infiltration of urethane resin. The coercivity was found to be 716.2 kA/m, and the remanence was ~0.3 T. Another powder-based AM technology laser powder bed fusion, or named SLS was also used to fabricate NdFeB-bonded magnets using a focused laser to melt the polymeric binder polyamide (PA) 12 powders added to NdFeB particles [105]. The magnetic properties of samples were affected by processing parameters, including laser power, hatch

Table 1 A summary of 3D printing techniques of magnetic materials

Category	Method	Material	Approximate resolution	Advantage	Limitation	Ref.
Vat photo-polymerization	SL	Bonded NeFeB, Sr ferrite	> 5 μm	High resolution; good surface quality	Particle sedimentation; low multi-material ability	[142,143]
	DLP	Magneto-responsive materials	> 5 μm	High resolution	Particle sedimentation; strong light scattering	[56,103]
	CLIP	Magnetic photopolymerizable resin	> 100 μm	High resolution; high printing speed	Particle precipitation; strong light scattering	[69]
	2PP	Superparamagnetic composite	> 100 nm	High resolution	Limited building size	[104]
Powder bed fusion	SLS	Bonded NeFeB	> 100 μm	Reuse of powders	Thermal stresses	[105,142]
	SLM	NeFeB, FeNi, FeSi	> 100 μm	High build speed	Removal of excess powders; residual stresses	[106,144,145]
BJ	BJ	Bonded NeFeB, FeSi	> 100 μm	Self-supported structures	Low density; poor surface finishing	[64,146]
Material extrusion	FDM	Bonded NeFeB, Ba ferrite, Sr ferrite	> 100 μm	Cost-effective	Limited surface finishing; poor mechanical properties	[57,65,119, 142,147–150]
	DIW	Bonded NeFeB, NeFeB, Ba ferrite, Sr ferrite, Fe_3O_4	1–400 μm	Multiple or graded materials; cost-effective	Clogging of small nozzles	[58,68,70, 151–153]
Magnetic-assisted 3D printing	DIW	Magnetic composites	1–400 μm	Particle alignment	Low resolution	[36,134]
	DLP	Magnetic composites	> 5 μm	Particle alignment	Particle sedimentation	[65,102,138,139]
	Inkjet printing	Magnetic composites	> 10 μm	Particle alignment	Easy clogging of printing heads	[141]

Table 2 Magnetic properties of 3D-printed permanent magnets

Material	Method	Binder	Density (g/cm^3)	M_r (T)	H_c (kA/m)	$(BH)_{max}$ (kJ/m^3)	Ref.
Bonded NdFeB	BJ	—	3.47	0.30	716.2	—	[64]
Bonded NdFeB	BJ	Diethylene glycol (DEG)	4.3	0.31	1345	—	[146]
Bonded NdFeB	SLS	Polyamide 12	3.6	0.30	708.3	15.3	[105]
Bonded NdFeB	FDM	Polyamide 11	3.57	0.31	740	—	[57]
Bonded NdFeB	BAAM	Polyamide 12	4.8	0.51	688.4	43.49	[63]
NdFeB (with $SrFe_{12}O_{19}$)	DIW	Epoxy resin	3.78	0.444	740.1	33.73	[58]
Bonded NdFeB	SLA	Polyfunctional methacrylates	4.83	0.388	734.7	—	[142]
NdFeB	SLM	No	7.0 (92%)	0.59	695	45	[106]
Ba ferrite	DIW	Polyvinyl alcohol (PVA)	4.14 (76.7%)	—	159.2	—	[152]
Ba ferrite	DIW	PVA	~4.51	—	316.01	17.83	[68]
Ba ferrite	FDM	Acryl butadiene styrene (ABS)	—	0.047	29	35	[148]
Sr ferrite	DIW	PVA	~4.65	—	386.06	19.98	[68]
Sr ferrite	DIW	Hydroxyethyl methacrylate	5.34 (97%)	0.383	271.2	26.34	[153]
Sr ferrite	FDM	Polyamide 12	—	0.213	244.69	—	[150]
Sr ferrite	FDM	Polyamide 6	2.861	0.201	162	—	[59]
Sr ferrite	FDM	Polyamide 12	2.962	0.22	281	—	[59]
SmFeN	FDM	Polyamide 12	3.404	0.308	565	—	[59]
Sr ferrite	Injection molding	A suitable binder	Nearly full density	0.384	256.3	—	[7]
Sr ferrite	Compaction	No	—	—	301	26	[10]

Note: The conversion for magnetic units: 10 kG = 1 T; 1 Oe = 79.6 A/m; 1 MGOe = 7.96 kJ/m^3, and B(G) = H (Oe) + 4π·M (emu/cm^3).

spacing, and layer thickness. After optimization, the maximum density was 3.6 g/cm^3 with a coercivity of 708.3 kA/m and a remanence of 0.3 T.

In some cases, ink-based 3D printing of NdFeB-bonded magnets have widely been explored. As an example, FDM printer was used to fabricate polymer-

bonded magnets with specific magnetic properties, which was evaluated by scanning the field of the printed magnet. The density of nylon-bonded NdFeB magnet reached 3.57 g/cm^3 with M_r = 0.31 T and H_c = 740 kA/m [57], which is lower than that of the molded samples. Moreover, big area additive manufacturing (BAAM) is a rapid and efficient extrusion-based 3D printing method for the large scale production of isotropic NdFeB-bonded magnets with high magnetic performance. The starting materials were mixtures of NdFeB powders and nylon-12 as the binder, and then printed by using an apparatus comparable to an FDM system [63]. The density of the final magnet was improved with the excellent magnetic properties (M_r = 0.51 T, H_c = 688.4 kA/m, and $(BH)_{max}$ = 43.49 kJ/m^3 (5.47 MGOe)) in comparison with traditional injection molded magnets. It is possible to manufacture large-scale objects using the BAAM method; however, the printing of fine structures is extremely difficult resulting from the large nozzle size.

DIW has also been widely utilized to manufacture bonded NdFeB magnets with complex geometry [58,151,156]. In this approach, a printable ink was composed of anisotropic NdFeB magnet particles with a solid loading of 40 vol% uniformly dispersed in epoxy resin matrix. Subsequently, the as-printed samples were cured at mild elevated temperature [151]. Nevertheless, effects should be made to improve the magnetic loading and thus obtain high-performed bonded magnets with controlled anisotropy. A novel UV-assisted direct write technique that combines extrusion and *in situ* curing was explored to fabricate magnets at room temperature as depicted in Fig. 5(a) [156]. The printable ink was created by dispersing NdFeB powders in a UV-curable polymer binder. The maximum solid loading was 60 vol%, and the as-printed magnets exhibited a remanence of 0.38 T and an intrinsic coercivity of 756.2 kA/m. This high value of coercivity resulted from the low processing temperature, which preserves the intrinsic coercivity of the raw material. It is worth noting that the magnetic performance should be further improved by the optimization of raw material, binder, printing conditions, etc. Additionally, SL can be used to print bonded NdFeB with a superior surface quality as well as a minimum features size of 0.1 mm in Fig. 5(b) [142]. Powders with a spherical morphology were preferred to optimize the printing quality. The printed magnets exhibited a remanence of 0.388 T and a coercivity of 734.7 kA/m, which were compared with magnets produced by FFF and SLS [142].

Although bonded magnets using binders have been widely printed, investigations were also performed to net shape parts without any binder to improve the remanence and consequently energy product. SLM was used to print net-shape NdFeB permanent magnet with stable magnetic performance [106]. Commercially available MQP-S powders supplied by Magnequench Corporation were used as raw materials. The spherical powders were selected to enable powder flowability for homogenous and dense deposition of a powder bed. The schematic illustration, hysteresis curve, and printed parts are depicted in Fig. 5(c) [106]. Using a laser output of 120 W and a layer thickness of ~20 μm, the magnetic properties of the as-printed NdFeB permanent magnet reached M_r = 0.59 T, H_c = 695 kA/m, and $(BH)_{max}$ = 45 kJ/m^3. It can be explained by the fact that the average grain size was ~1 μm, which had a positive influence on the intrinsic coercivity since it approaches the mono-domain limit of the NdFeB phase. However, it is still challenging to precisely control the grain size, porosity, and oxidation in the printed magnets for achieving desired magnetic properties by using SLM [116].

4.1.2 Hard ferrite ceramic materials

The production of hard ferrites is also of great interest because of combining benefits of 3D printing and the use of ceramics in high frequencies [59,68,152]. Such alternatives to rare earth permanent magnets may decrease the cost for applications as electrical motors. Our group successfully produced barium ferrites by DIW and evaluated the magnetic properties [152]. Relying on a paste composed of $BaCO_3$ and Fe_2O_3 powders dispersed in aqueous binder solution, parts have been printed with a layer height of 0.6 mm, a printing speed of 5 mm/s, and sintered at temperatures ranging from 1000 to 1400 ℃ for the phase formation as well as densification as illustrated in Fig. 6(a). The hysteresis loop is depicted in Fig. 6(b), demonstrating a typical hard magnetic sample with $H_c \approx 160$ kA/m. As could be expected, higher temperatures favor pore elimination and densification, whereas leading to a drastic decrease in the coercivity as a result of large grain size. This technology provides the possibility of fabricating hard ferrites with complex structures as shown in Fig. 6(c).

To further improve the coercive field, precursor powders were subjected to mechanical milling instead of un-milled counterparts in the following studies [68]. Notably, the value of the coercivity can be effectively

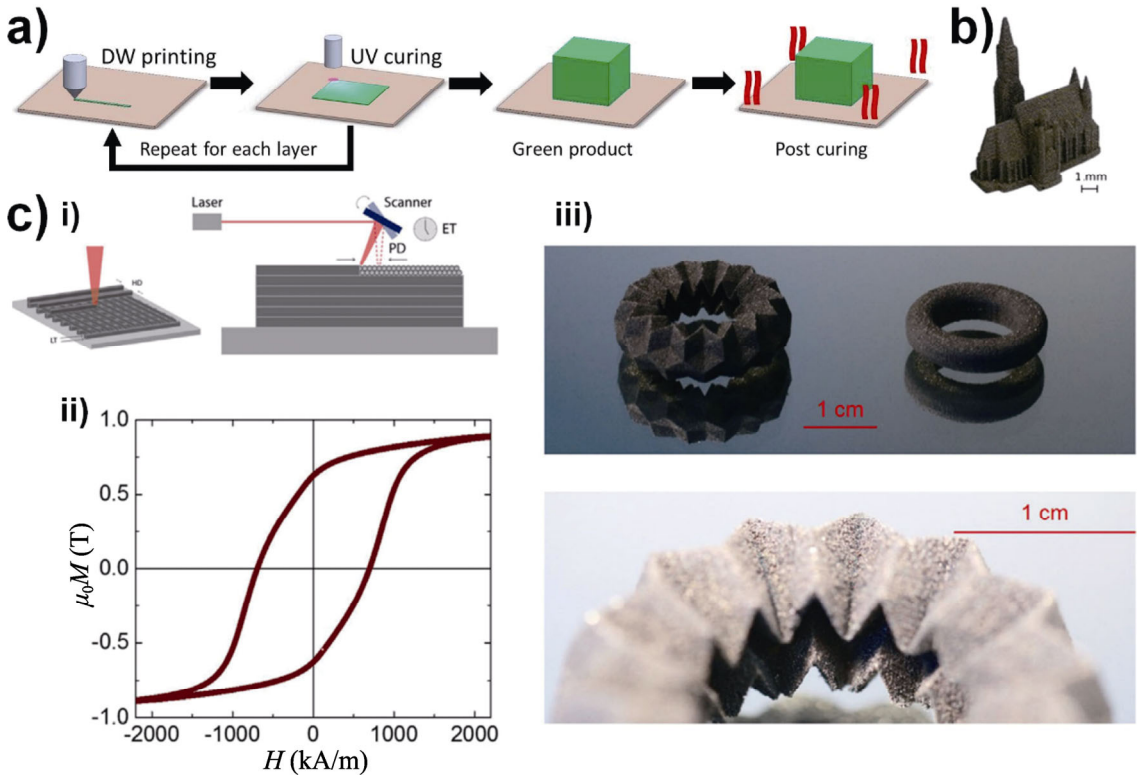

Fig. 5 (a) Schematic diagram of the UV-assisted direct write process. Reproduced with permission from Ref. [156], © Elsevier B.V. 2018. (b) 3D-printed magnets. Reproduced with permission from Ref. [142], © the authors 2020. (c) 3D-printed permanent magnet. Reproduced with permission from Ref. [106], © WILEY-VCH Verlag GmbH & Co. KGaA, Weinheim 2017.

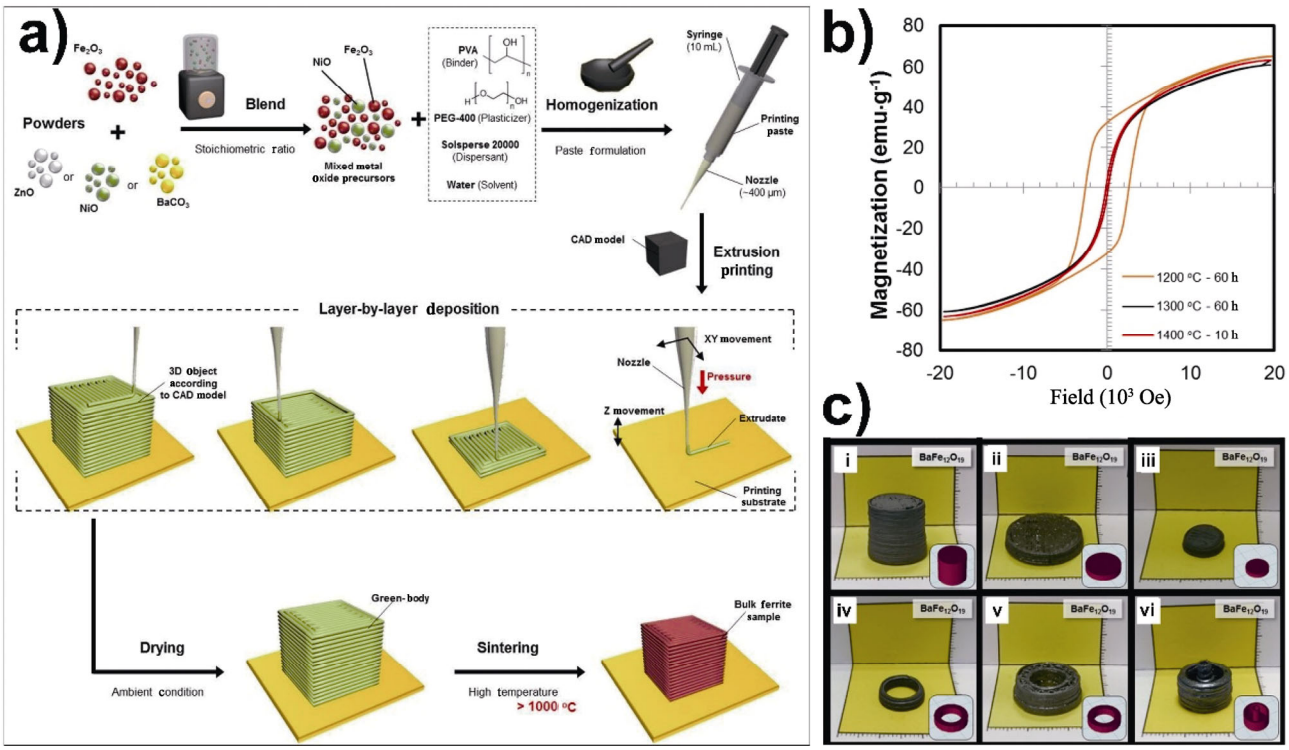

Fig. 6 (a) Schematic diagram showing the process of extrusion free forming (EFF); (b) magnetic hysteresis loops of the 3D-printed $BaFe_{12}O_{19}$; (c) digital photographs of 3D-printed $BaFe_{12}O_{19}$. Reproduced with permission from Ref. [152], © The Royal Society of Chemistry 2017.

improved when compared to untreated powders by the conventional ceramic processing. More importantly, the $(BH)_{max}$ of the resultant barium ferrites reached 17.83 kJ/m^3 after sintering at 1150 ℃ with hysteresis loop depicted in Fig. 7(a). It is presumably contributed to the fine milled powders and the optimized thermal treatment for grain growth. In a word, 3D printing of barium ferrites derived from milled powders is a promising candidate for producing magnets with remarkable magnetic properties. In addition, nanosized barium ferrite dispersed in acryl butadiene styrene (ABS) matrix can be printed by FFF [148]. However, an increasing of voids inside the filament occurred with the increase of solid loading. Sukthavorn *et al.* [157] also used FDM technology to fabricate poly(lactic acid)/barium ferrite with different ratios as digital photographs and magnetic properties as demonstrated in Fig. 7(b). Interestingly, the results showed that silane-modified barium ferrite can improve homogeneity between the ceramic filler and polymer matrix; however, the magnetic properties were not obviously altered after adding silane. These attempts enhanced the magnetic properties of 3D-printed magnetic materials, unleashing great potential in wide applications.

Strontium ferrite ($SrFe_{12}O_{19}$) is also a notable hard magnetic material due to its additional advantages, such as comparatively low cost, wide availability, and strong magnetocrystalline anisotropy. Starting from milled precursor powders, net-shape strontium ferrite was manufactured by DIW technique in our group. After the optimization of annealing process, the coercivity reached up to 386 kA/m as the hysteresis loop depicted in Fig. 8(a) (the inset shows the 3D-printed ferrites) [68]. Still in the context of Sr ferrites, complex-shaped part has been fabricated by using 3D gel-printing as depicted in Fig. 8(b) [153]. Based on the hydroxyethyl methacrylate slurry, strontium ferrite was continuously extruded at a speed of 20 mm/s with a layer height of 0.2 mm [153]. After sintering at 1300 ℃, the resultant ferrites presented a density of ~5.34 g/cm^3 with an excellent magnetic performance: M_r = 0.383 T, H_c = 271.2 kA/m, and $(BH)_{max}$ = 26.34 kJ/m^3. The appearance, surface morphology, and several complex-shaped strontium ferrite samples are demonstrated in Figs. 8(c), 8(d), and 8(e), respectively [153]. It was demonstrated that the 3D-printed samples had good surface quality and dimensional stability after sintering, indicating that 3D printing technology can be employed to produce hard ferrite ceramics.

Importantly, the impact of an external magnetic field was investigated during the printing process [59,143,150]. Nagarajan *et al.* [143] developed particle alignment configuration for material jetting 3D printing process using real-time optical microscopy as indicated in Fig. 9(a). It was resulted from permanent magnets capable of generating a magnetic field to align strontium ferrite hard magnetic particles in the liquid resin. Moreover, it was observed that the orientation of magnetic particles was determined by the distance of permanent magnets and the magnetization time. In some cases, magnetic particles can also be aligned by applying an external magnetic field during the FFF process. As the thermoplastic polymer matrix melts, the magnetic particles can orient under the external magnetic field. Also, mechanical orientation over the printing direction was available during the printing process as depicted in Fig. 9(b) [59]. Meanwhile, the feedbacks and some3D-printed ferrites with complex structures were

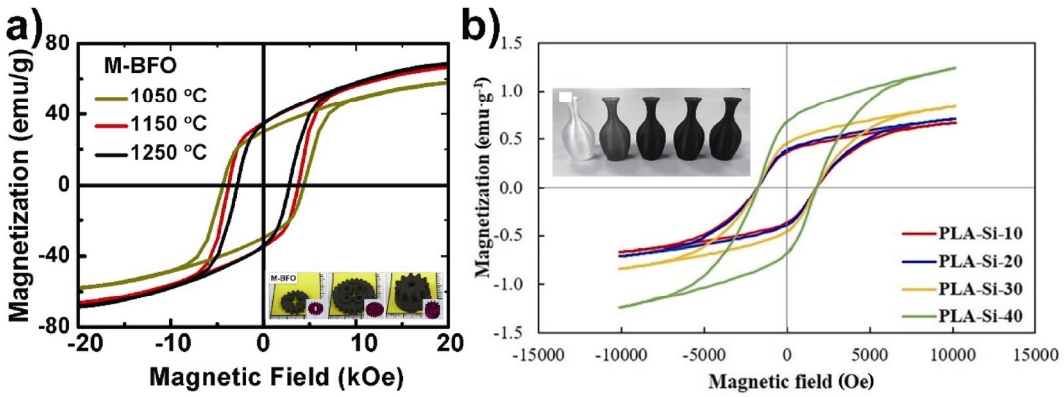

Fig. 7 (a) Magnetic hysteresis curves of the 3D-printed barium hexaferrite (M-BFO); the inset shows the digital photographs of ferrites after calcinations. Reproduced with permission from Ref. [68], © Elsevier B.V. 2019. (b) Magnetic hysteresis curves of treated-silane barium ferrite; the inset shows the digital photographs of 3D-printed magnetic composite filament $BaFe_{12}O_{19}$ content at 0, 10, 20, 30, and 40 phr. Reproduced with permission from Ref. [157], © Wiley Periodicals LLC 2021.

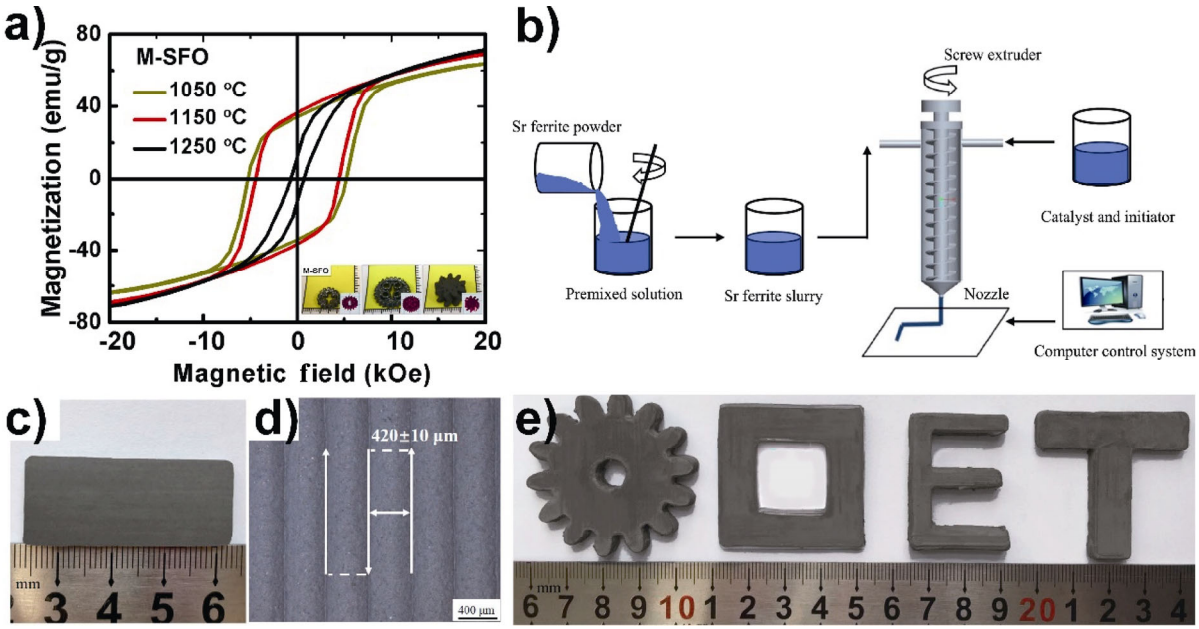

Fig. 8 (a) Magnetic hysteresis curves of the 3D-printed strontium hexaferrite (M-SFO); the inset shows the digital photographs of ferrites after calcinations. Reproduced with permission from Ref. [68], © Elsevier B.V. 2019. (b) Schematic diagram of the 3D gel printing process; (c) sintered strontium ferrite sample; (d) surface morphology of sample; (e) strontium ferrite parts prepared by the 3D gel printing. Reproduced with permission from Ref. [153], © Elsevier Ltd and Techna Group S.r.l. 2018.

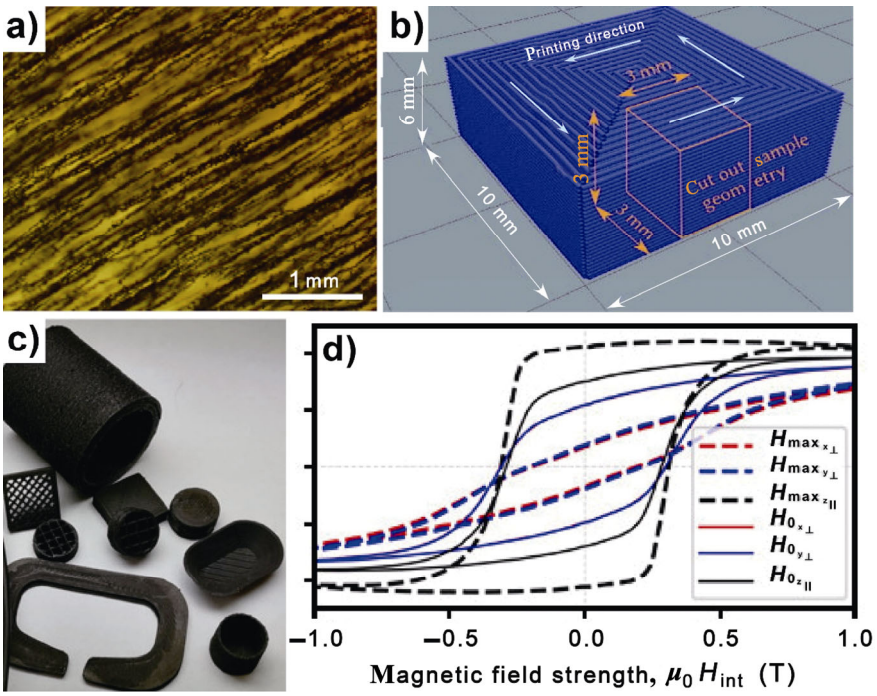

Fig. 9 (a) Micrographs of magnetic particles in liquid resin rotate with angular orientation of 30°. Reproduced with permission from Ref. [143], © Elsevier B.V. 2018. (b) Every sample is printed in the direction of the light blue arrows. The sample for measurement is printed in the same direction. Reproduced with permission from Ref. [59], © Author(s) 2020. (c) Picture of the filament and several 3D-printed samples; (d) hysteresis measurements for isotropic (no external field) and anisotropic (maximum external field) printed magnets in all magnetization directions. Filling fraction was 55 vol%. Reproduced with permission from Ref. [150], © Author(s) 2020.

demonstrated in Fig. 9(c) [150]. Fortunately, it was observed that strontium ferrite particles can be aligned during printing the anisotropic structures with a significant increase of the remanence compared to

samples without an external field as shown in Fig. 9(d) [150]. These aligned magnetic particles during the 3D printing process in the presence of an external magnetic field can promote the creation of complex structures with high permeability.

4. 2 Soft magnetic materials

Similar to the field of permanent magnets, 3D printing of soft magnetic materials has been widely explored due to their primary importance in magnetic devices, such as transformers, sensors and motors. In this area, efforts target the development of materials combining a high M_s with the minimization of the hysteresis loop area via the reduction of the intrinsic coercivity.

4.2.1 Soft magnetic alloys

An important family of soft magnetic materials referring to FeNi alloy has been manufactured using high-powered laser SLM and LENS techniques [158]. By using SLM, it has been realized that the magnetic properties of Fe–30%Ni were strongly influenced by the laser parameters [144]. As can be observed for Fe–30%Ni, the lowest H_c is 88 A/m, and the highest magnetization M_s is 565 Am^2/kg with a combination of laser scanning velocity of 0.4 m/s and laser power at 110 W, which can be attributed to the solid solution Fe_3Ni_2 formation with grain refinement [144]. Further evaluation of FeNi-based alloys using LENS has also been reported, including FeNi, NiFeV, and NiFeMo due to the excellent permeability and reasonable M_s [159]. The microstructural evolution, phase formation, and magnetic performance of these alloys were investigated and affected by the processing parameters, such as laser power and scanning speed. When compared to those of conventionally processed counterparts, the H_c values were higher for the laser processed alloys, which can be attributed to the microstructural defects [107].

Among soft magnetic materials, FeSi alloy occupies a prominent position due to its wide applicability in transformers, industrial motors, and other electromagnetic devices. In some cases, Fe–6.9 wt%Si parts were printed by using SLM [145]. Starting from pre-alloyed powders, near-fully dense FeSi alloy 3D parts were manufactured using SLM. It was observed that the as-built sample had a <001> crystallographic texture along the build direction of samples by increasing the energy input. To minimize energy losses and eliminate the effect of residual stresses, high-temperature post-annealing was applied to the as-built FeSi samples to cause grain enlargement [160]. It was shown that annealing retained the SLM-induced <001> crystallographic texture of the grains along the build direction. In this perspective, texture has been identified as the main drivers that affect magnetic properties.

Similarly, a significant effort has been made to realize solid net shape parts of soft magnetic materials using LENS 3D printing method, such as $(Fe_{60}Co_{35}Ni_5)_{78}Si_6B_{12}Cu_1Mo_3$ (type Finemet) [161]. It was demonstrated that the semi-hard magnetic characteristics in $(Fe_{60}Co_{35}Ni_5)_{78}Si_6B_{12}Cu_1Mo_3$ samples can be regulated by adjusting laser power [161]. These results demonstrated that the laser-based AM had the ability to process soft magnetic alloys and tune the microstructure and magnetic performance as a function of processing parameters and compositions.

4.2.2 Soft ferrite ceramic materials

3D printing opens new possibilities to create complex-shaped soft ferrite parts given the low cost of materials and the indispensable role in various aspects of electronics especially in high frequencies. Ni and NiZn ferrites have been manufactured by using DIW in our previous works [50,152]. In the presence of water-soluble binder and plasticizer, a paste composed of NiO and Fe_2O_3 powders was extruded at room temperature, subsequently the as-printed sample was annealed at high temperatures ranging from 1000 to 1400 ℃ [152]. As the hysteresis loop depicted in Fig. 10(a), it was demonstrated that Ni ferrite exhibited typical soft magnetic behavior with high degree of M_s which influenced by annealing temperature. Magnetic structures with unique geometries (e.g., ring, hollow cube, and mesh present in Fig. 10(b)) were obtained. This technique can be readily extended to other functional ferrites or ceramics simply by changing the metal oxide powder precursors. For example, NiZn ferrites with remarkable soft magnetic properties were printed using the same method in our work [50]. The prepared magnetic rectangular mesh after calcination depicted in Fig. 10(c) was characterized comprehensively. It was observed that a fully dense structure can be obtained resulting from the homogeneous shrinkage. Furthermore, SEM microstructures and crystalline phases were investigated in Figs. 10(d) and 10(e), respectively. It was found that the soft ferrite had polycrystalline micro-sized grains with no presence of pores, and pure inverse spinel structure was obtained. Additionally, magnetic properties of mesh were evaluated

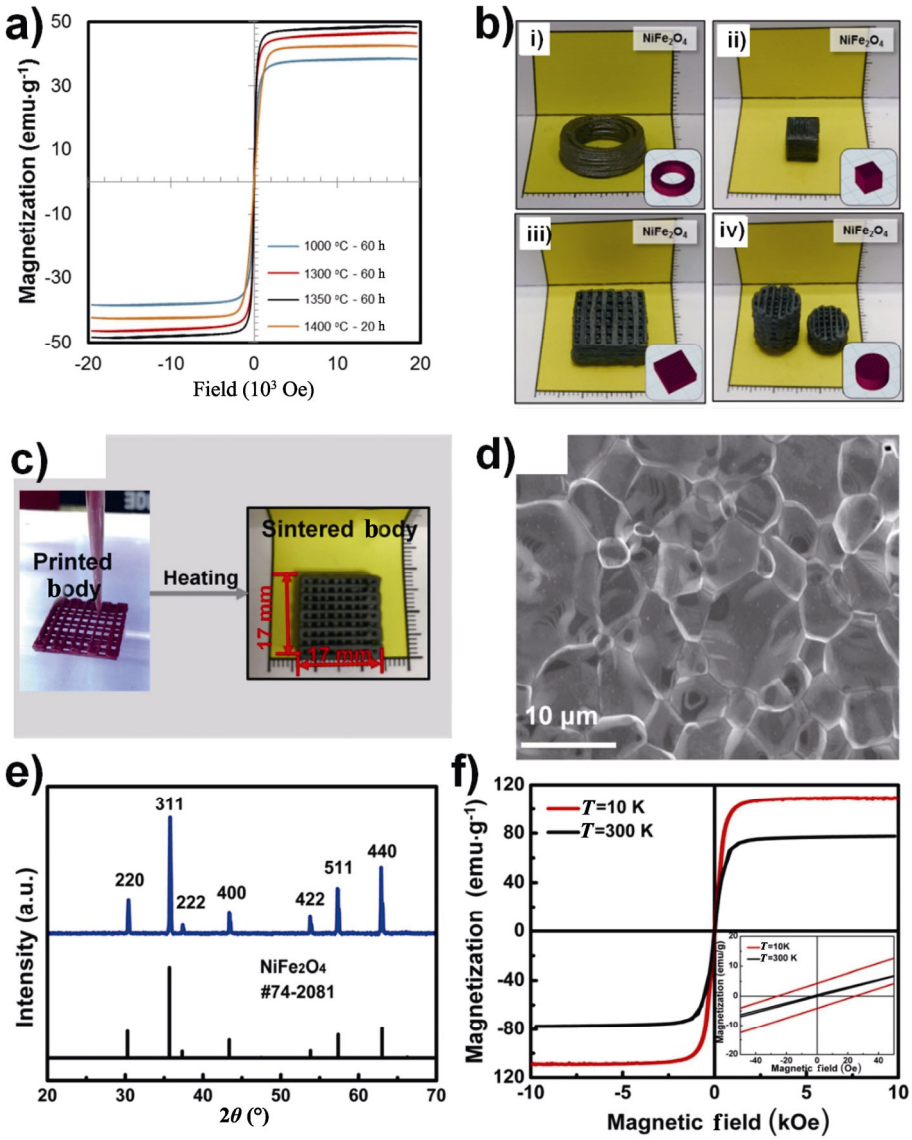

Fig. 10 (a) Magnetic hysteresis loops of the 3D-printed $NiFe_2O_4$ sintered under different conditions; (b) digital photographs of the 3D-printed $NiFe_2O_4$. Reproduced with permission from Ref. [152], © The Royal Society of Chemistry 2017. (c) Digital photographs of the as-printed and sintered body of ferrite filter with mesh structures; (d) SEM microstructures of the magnetic filter; (e) XRD pattern of the fabricated filter; and (f) magnetic hysteresis loops at 10 and 300 K. Reproduced with permission from Ref. [50], © American Chemical Society 2017.

using a superconducting quantum interference device as shown in Fig. 10(f). It was demonstrated that M_s was as high as 77.5 emu/g at room temperature with near zero coercivity and zero remanence from magnetic hysteresis loops. Therefore, soft ferrite with intricate structures and excellent soft magnetic properties can be produced by extrusion-based 3D printing.

Similarly, An *et al.* [162] also utilized DIW technology to print soft NiZn ferrites. It was demonstrated that the rheological properties of the ceramic suspensions determined flowability (printability), height, and the overhang angle. The magnetic properties for 3D-printed toroidal samples exhibited a typical soft magnetic characteristic as depicted in Fig. 11(a) [162]. In this way, a transformer core with an EFD design was successfully 3D printed in Fig. 11(b) [162]. More impressively, Liu *et al.* [163] pointed out that the ability to retention the original shape was an important factor for paste 3D printing as shown in Fig. 11(c). As we can see, the ferrite sample retained its shape and began to sag when the height reached 12 mm. With the exploration of slumping models, a guideline was developed to print the slump-free ferrite core structures as demonstrated in Fig. 11(d) [163]. Clearly, the heights of the printed

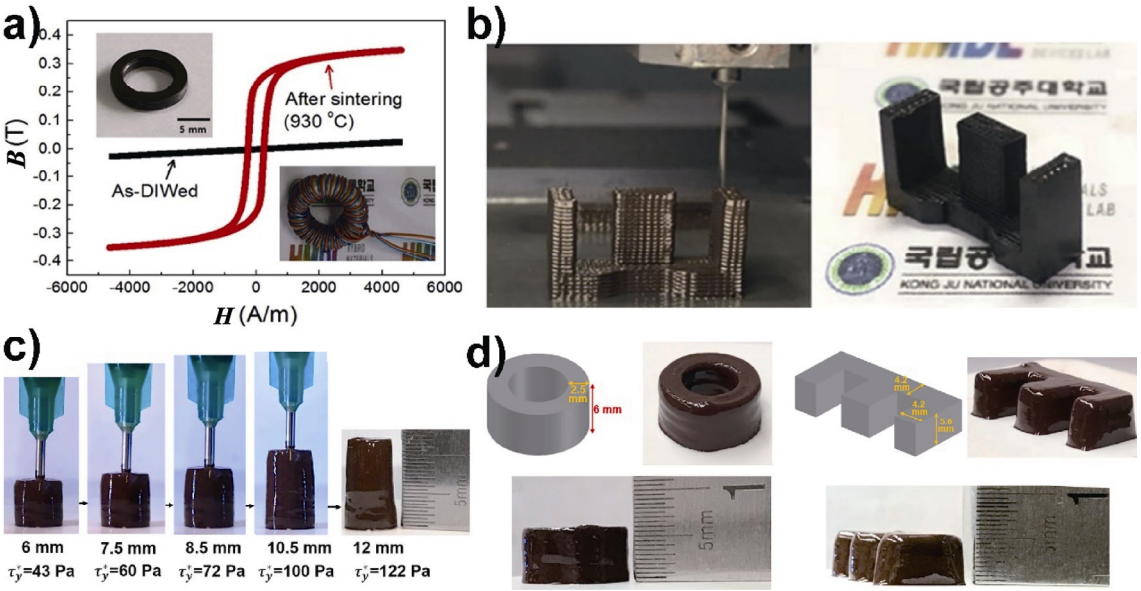

Fig. 11 (a) Magnetization hysteresis curves of the 3D-printed NiZn–ferrite toroid samples before and after sintering; (b) 3D-printed magnetic core. Reproduced with permission from Ref. [162], © Elsevier Ltd and Techna Group S.r.l 2019. (c) Printing a cylinder using ferrite paste with different yield stress; (d) demonstration of an as-printed toroid core and an as-printed E core. Reproduced with permission from Ref. [163], © Elsevier Ltd and Techna Group S.r.l 2020.

structures matched well with the designed heights. Furthermore, Liu *et al.* [164,165] also demonstrated soft NiCuZn ferrite with different or tailorable permeability by controlling the fractions of additives during extrusion-based 3D printing, such as cobalt oxides and silica particles. It should be noted that other element doping is promising to improve magnetic properties in the future [166,167].

Moreover, DIW technique was also employed to print other soft magnetic ceramics, such as iron oxide [70]. With this method, different shapes of cores, such as rectangular shape, toroidal shape, and porous lattice structure can be printed as depicted in Fig. 12(a). To study the influence of additives on magnetic properties, magnetic hysteresis loops of particles and the ink were compared in Fig. 12(b). It was observed that both samples exhibited similar magnetic behavior, confirming that the additives did not affect the magnetic property of particles. Expectedly, the printed structure can be used as the cores in inductors to enhance the inductance as depicted in Fig. 12(c). This aqueous ink system has shown significant potential for domestic printing of ceramics.

More interestingly, FDM was utilized to print magnetic materials. Aqzna *et al.* [168] printed Zn ferrite by dispersing particles in ABS filament with the fabricating process presented in Fig. 13(a). The influence of filler content was also studied. Similarly, Wang *et al.* [169] utilized FDM to print NiZn ferrite with complex lattice structures as shown in Fig. 13(b). In the end, inkjet printing is a method to print ferrite film using low-viscosity inks. With this method, NiZn ferrite film with a trench structure was first inkjet-printed to reduce the resistive loss of the coil as illustrated schematically in Figs. 13(c) and 13(d) [170].

4. 3 Magnetic composites

Magnetic composites combine the nonmagnetic matrix and magnetic particles, achieving a system with functional properties which cannot be attained by any of the material alone [171–173]. Still in the scope of manufacturing, it is worth mentioning that such composites can be usually printed by using liquid polymers/resins filled with magnetic particles that can be cured based on SL [102,174], or be extruded in the form of filament by FDM [78,175–177], DIW [36,62,178,179], and inkjet printing [141,180].

In the fabrication of magnetic composites using SL-related approaches, the printing process usually starts with directly loading magnetic particles within the liquid photopolymer matrix. Subsequently, the mixture is polymerized by a laser beam or patterned light in a layer-by-layer fashion. Credi *et al.* [181] printed cantilever-based magnetic microstructures by means of SL, and the structures exhibited excellent sensing and actuating performances when an external magnetic field was

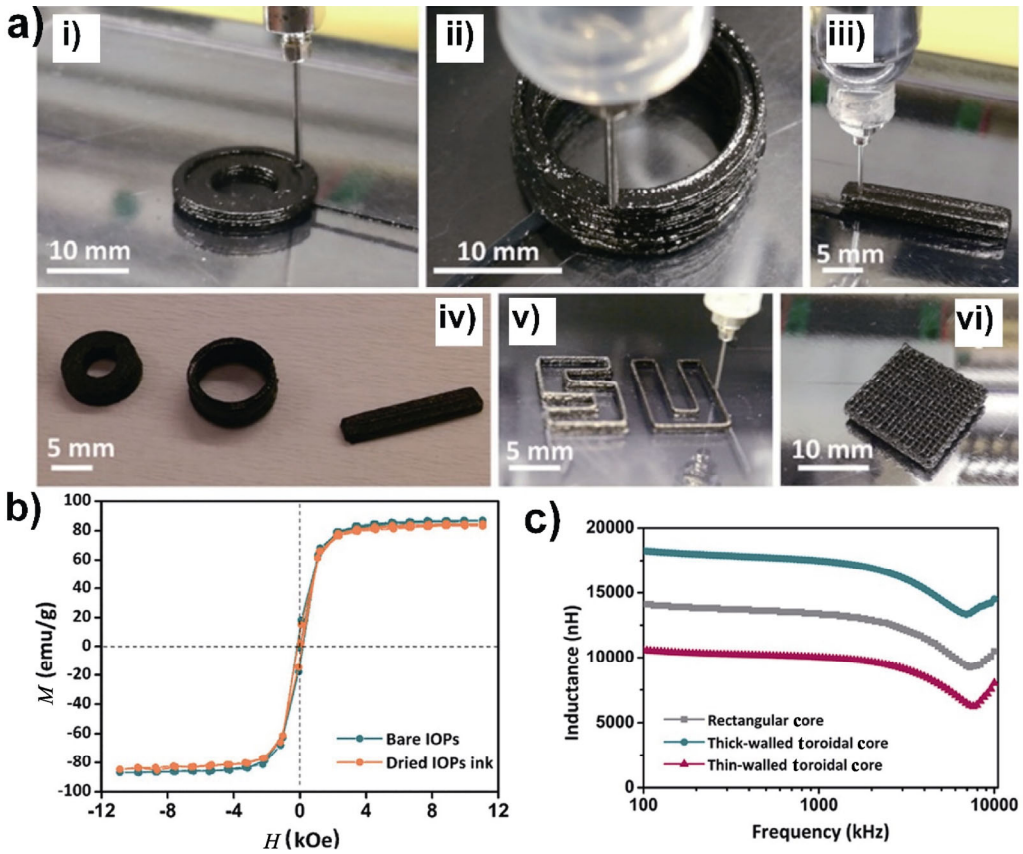

Fig. 12 (a) 3D printing of the magnetic structures; (b) magnetic hysteresis loops of the ink; (c) frequency response of the inductance. Reproduced with permission from Ref. [70], © American Chemical Society 2018.

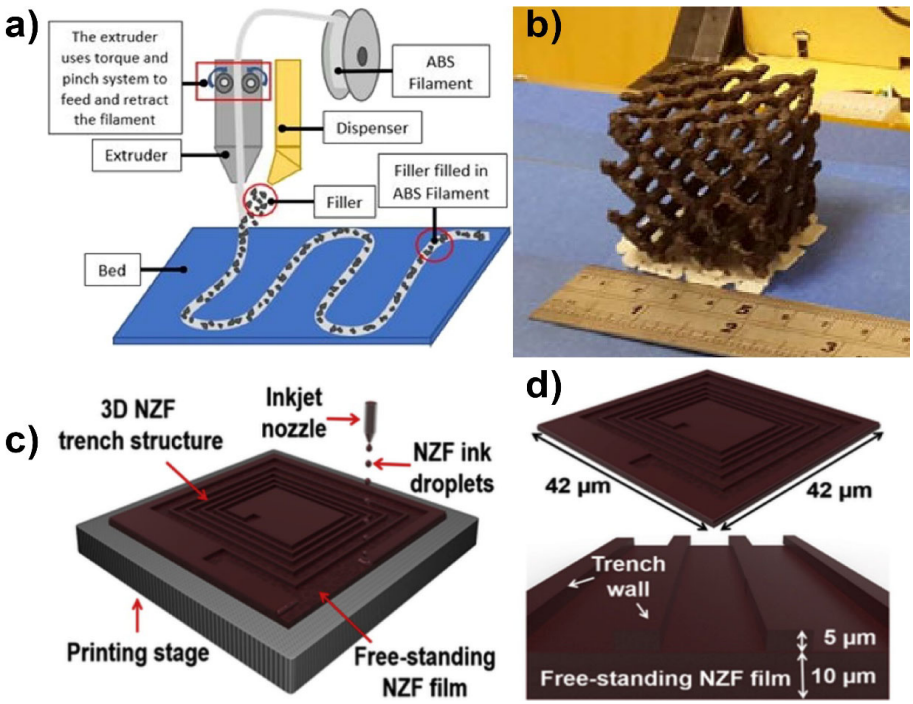

Fig. 13 (a) Fabrication process. Reproduced with permission from Ref. [168], © Society of Plastics Engineers 2018. (b) Photograph of a 3D-printed lattice structure using 10 vol% NiZn ferrite filament. Reproduced with permission from Ref. [169], © The Materials Research Society 2015. (c) Schematic diagram depicting fabrication of 3D NiZn-ferrite (NZF) structure; (d) dimension of NZF structure. Reproduced with permission from Ref. [170], © Elsevier Ltd. 2019.

applied. Using the same method, magnetic composites based on magnetic nanoparticles and photopolymers with appropriate geometries were conducted [182]. Moreover, DLP is also used for printing magnetic nanocomposite materials. Among them, Lantean *et al.* [56] demonstrated the possibility to print magneto-responsive polymeric materials. The tunable magnetic properties of the samples were achieved by modifying the Fe_3O_4 nanoparticle loading. And the 3D structures exhibited different kinds of movements, such as shape-shifting and folding–unfolding using external magnetic fields as depicted in Figs. 14(a) and 14(b). Ji *et al.* [103] also showed the possibility of printing magnetic responsive and nonresponsive materials into one body by multi-material DLP technology in Fig. 14(c). At the end, 2PP was applied to print superparamagnetic composites with shape-independent magnetic properties [104].

Alternatives to vat polymerization 3D printing technology are FDM and DIW. As a first example, poly-metal soft magnetic composites were printed using FDM strategy [176]. The composites comprise polymer ABS as the matrix with 40 vol% stainless steel as the filler. At this high filler ratio, the composite exhibited stronger magnetic properties with reduced mechanical performance. In a word, the results can be useful in magnetic sensing applications. Further examples include 3D printing magnetic composite transformers using FDM method [78]. Using this strategy, thermoplastic composites filled with carbonyl iron particles were fabricated which can be used for radar wave absorbing [177].

Still in the form of filaments, magnetic composites can be extruded using DIW method. Zhu *et al.* [62] developed a new composite ink system composed of polydimethylsiloxane (PDMS) as flexible matrix component and soft magnetic iron nanoparticle fillers. The printed 3D composite structures can rapidly respond to magnetic stimulus as schematically shown in Fig. 14(d), which is called 4D printing. The fast response is attributed to Fe particles with excellent soft magnetic properties which could obtain or lose magnetization immediately depending on the external magnetic field. Impressively, Bastola *et al.* [183] demonstrated that DIW technique can be used to print iron powder-based magnetorheological elastomers that are a class of smart materials, whose properties can be controlled by applying an external magnetic field. During the printing process, every layer was a composite structure with the magnetorheological fluid encapsulated into an elastomer

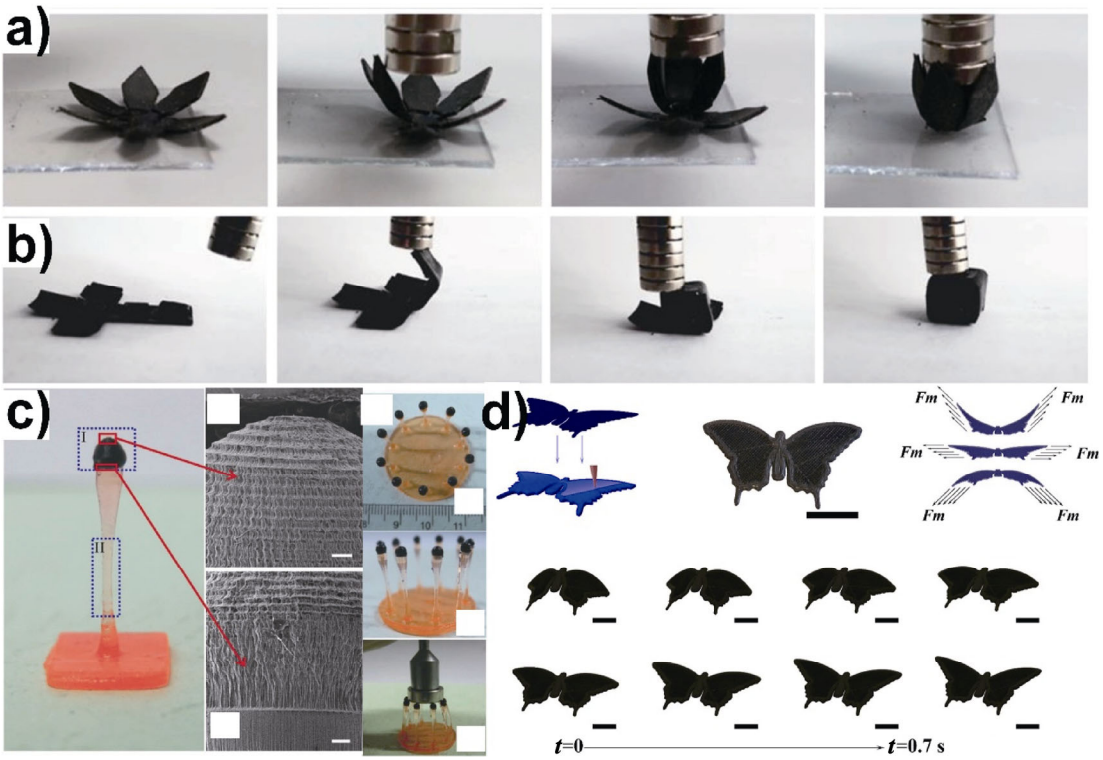

Fig. 14 (a) Printed magnetic flower; (b) 2D magnetic structure is able to create a 3D cube. Reproduced with permission from Ref. [56], © WILEY-VCH Verlag GmbH & Co. KGaA, Weinheim 2019. (c) Digital photo and SEM images of a 3D-printed structure. Reproduced with permission from Ref. [103], © WILEY-VCH Verlag GmbH & Co. KGaA, Weinheim 2017. (d) Schematic illustration and printed 3D butterfly. Reproduced with permission from Ref. [62], © American Chemical Society 2018.

matrix. Using this strategy, the hybrid elastomers were printed into different patterns [67,184]. Other researchers have also fabricated different arrays of magnetorheological elastomers using the extrusion-based 3D printing technique [185]. Moreover, Sindersberger *et al.* [186] also used this approach to investigate the possibilities of printing magneto-active polymers, which are composites comprising a polymer matrix and carbonyl iron powders.

Additionally, some researchers explored inkjet printing technique to print magnetic composites [141,187]. Song *et al.* [141] reported an inkjet printing method with magnetic alignment capability by an external magnetic field. The results demonstrated an increase in permeability and a decrease in hysteresis losses in the alignment-induced direction. Impressively, 3D inkjet-printed magnetic composites for electromagnetic applications were reported [188]. In summary, 3D printing has the possibilities to bring magnetic particles embedded into a polymer matrix, gaining momentum in the area of magnetic composites.

4. 4 Summary

Different magnetic materials and composites have been fabricated by using 3D printing approaches as illustrated in Fig. 15(a). For permanent magnets, mainly polymer-bonded NdFeB, BJ, SLS, SL, and extrusion-based FDM and DIW technologies are the most suitable. It is of significant interest to increase the volumetric fraction of magnetic powders and use starting materials with stronger magnetic properties. However, the main disadvantage of bonded magnets is the reduced energy product compared to sintered magnets due to the incorporation of the non-ferromagnetic polymer matrix. Therefore, net-shape NdFeB without the presence of binder was carried out by SLM technique. More interestingly, hard ferrite ceramics were printed by DIW starting from milled precursor powders with enhanced magnetic properties. Nevertheless, the assessment of 3D printing capability is still in fundamental stages of development.

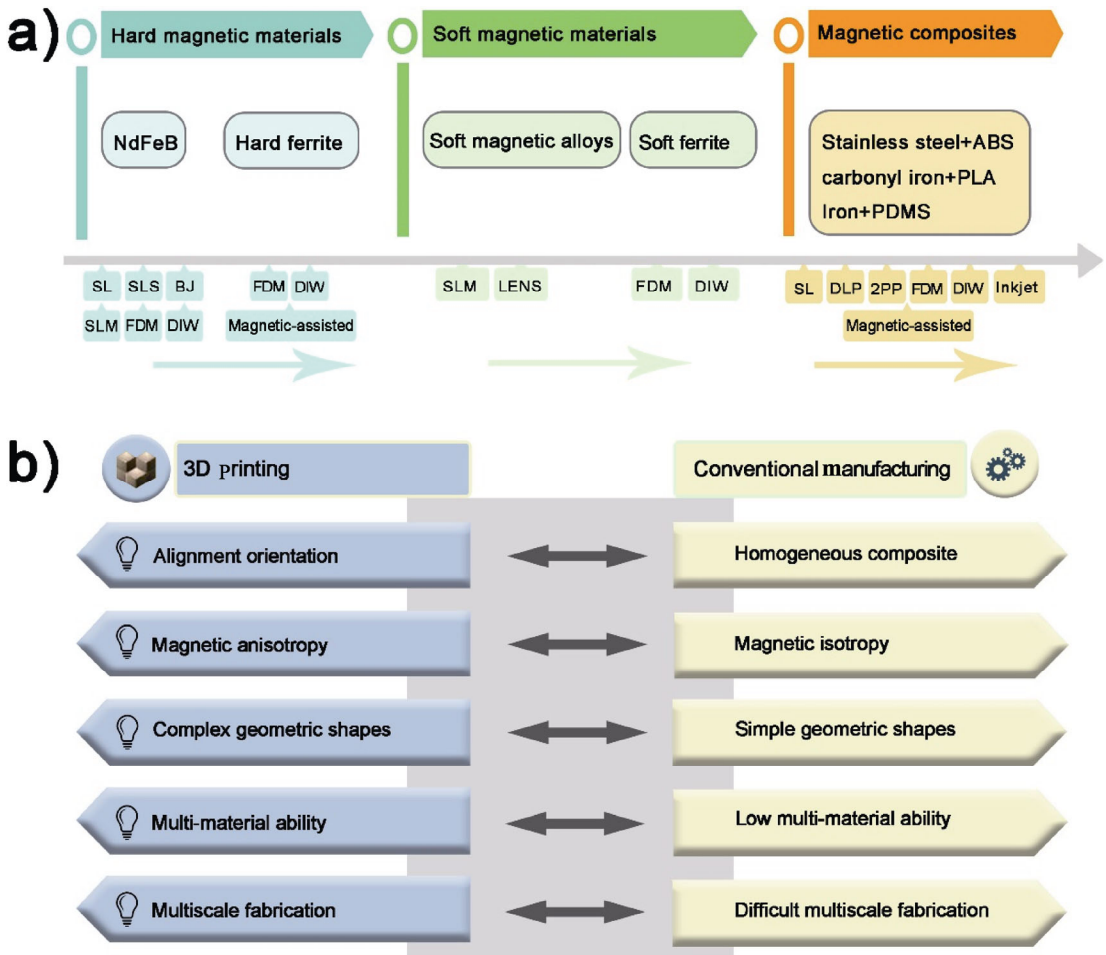

Fig. 15 (a) Summary of magnetic materials fabricated by various 3D printing techniques. (b) Comparison of 3D printing and conventional manufacturing.

Concerning soft magnetic materials, FeNi and FeSi alloys have been manufactured by utilizing high-power SLM and LENS techniques. Soft magnetic objects with dense structures and arbitrary shapes can be obtained, while the coercivities were higher than conventionally processed counterparts of similar compositions, presumably resulting from the microstructural defects. Therefore, the magnetic performance can be modified by the laser processing parameters, such as laser power, scanning speed, printing velocities, and interval time. Moreover, soft ferrites, such as Ni ferrites and NiZn ferrites, have been manufactured by DIW technique with high M_s. These results demonstrated that 3D printing had the ability to process soft magnetic materials, and their corresponding magnetic properties can be optimized by the modification of processing parameters. To print magnetic composites with flexibility, vat photopolymerization by dispersing magnetic particles in liquid resins, FDM, DIW, and inkjet printing approaches were commonly used.

Compared to conventional manufacturing techniques including injection molding and compression, 3D printing with the assist of magnetic field can fabricate anisotropic structures with magnetic alignment, which significantly affect the magnetic properties. Moreover, the advantages of 3D printing also lie in the fabrication of complicated multiscale structures with multi-material capabilities as shown in Fig. 15(b). Importantly, magnetic properties fabricated by 3D printing are comparable with materials conducted by conventional approaches as grey color marked in Table 2. However, traditional processing is complicated and time-consuming due to the requirements of molds and dies, resulting in magnetic isotropic structures with simple geometric shapes, which restricts the wide applications. In summary, 3D printing is able to conduct the functional magnetic materials with complex shapes and high performance, providing the possibility for wide applications.

5 Applications of 3D-printed magnetic materials

With 3D printing, it is possible to produce programmed magnetic materials in a predesigned way. These magnetically responsive materials can provide remote controllability and fast response capabilities [189,190]. Many research efforts have been focused on enriching the functionalities of 3D-printed magnetic materials. There are many noteworthy examples; here, limited by length, we pay attention to advances in printing soft actuators and robotics, transformers, energy harvester, electromagnetic microwave absorption, drug delivery, magnetic separation, and magnetic levitation. In this section, we will review these applications.

5.1 Soft robotics

Soft actuators and robots are improving human-machine interactions and driving innovations in myriad applications due to the capacity to perform movements with high degrees of freedom [191]. Unlike traditional robots composed of rigid materials, soft robots generally based on gels [192,193], elastomers [194], and other soft materials have the ability to adapt to the environment [195]. Moreover, soft robots can operate in a proper magnetic environment by incorporating magnetic particles into host polymer matrix [189], otherwise coating the magnetic materials on the surface of polymer scaffolds [196], However, it is difficult to incorporate multiple functionalities without complex geometries [197,198]. 3D printing enables the production of complicated structures with multi-material ability, and thus the advances in 3D printing have resulted in a significant development of soft systems [199].

To date, Joyee and Pan [139,200] printed an inchworm-inspired soft robot with the magnetic field assisted projection SL technique. This soft robot was made of magnetic particle-polymer composites and capable of linear and turning movements as illustrated in Fig. 16(a) [139]. With different modes of locomotion, the untethered magnetic actuation robot is promising in a controlled drug delivery application (Fig. 16(b)) [139].

Moreover, a few studies have been conducted on 3D-printed magnetic actuators [103,179]. Ji *et al.* [103] fabricated a soft magnetic actuator using multi-material DLP printing. As a case study, a flexible gripper was printed by the integration of magnetic and nonmagnetic materials into one body. The printed gripper can be actuated to grab the targeted object due to magnetic attraction as shown in Fig. 16(c). Roh *et al.* [179] demonstrated the printing of intelligent soft actuators by direct writing with homo-composite silicone ink. The architectures can possess programmed magnetic responsiveness with complex functions when applied magnetic fields, while capturing an object floating on water was depicted in Fig. 16(d). Instead of magnetic composites by embedding magnetic particles in a polymer matrix, ferrofluid-based soft actuators can also be 3D

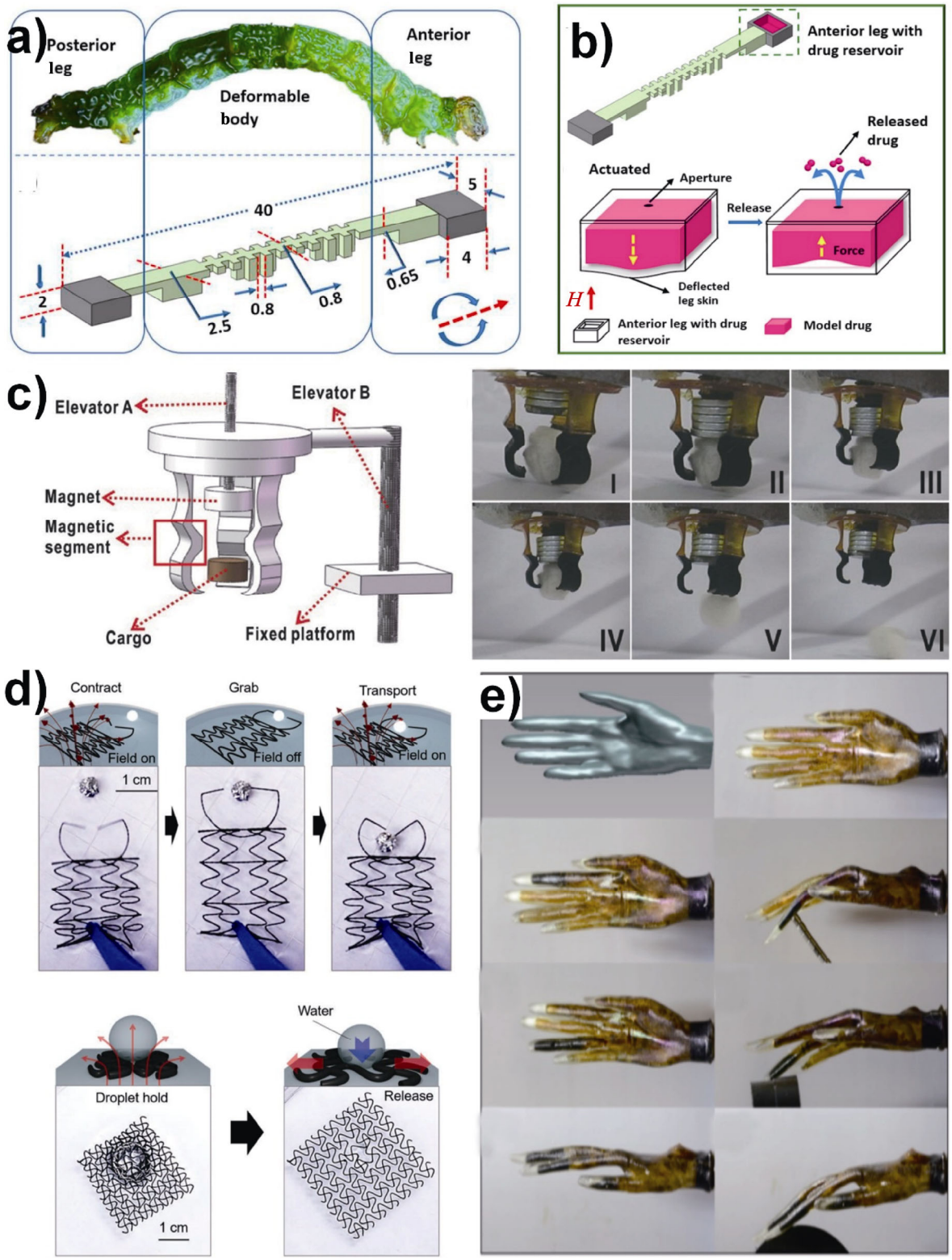

Fig. 16 (a) Design of the composite soft robot; (b) design of drug reservoir and drug release. Reproduced with permission from Ref. [139], © The Authors 2019. (c) Schematic illustration and demonstration of the 3D-printed gripper. Reproduced with permission from Ref. [103], © WILEY-VCH Verlag GmbH & Co. KGaA, Weinheim 2017. (d) Extensible surface grabber and magnetically responsive water droplet dispenser. Reproduced with permission from Ref. [179], © WILEY-VCH Verlag GmbH & Co. KGaA, Weinheim 2019. (e) Illustration and images of a hand with a magnetic ferrofluid reservoir. Reproduced with permission from Ref. [201], © IEEE 2019.

printed [201]. In this work, the hand-like actuator with remote magnetic actuation can move to different locations by the distribution of ferrofluid from a reservoir in Fig. 16(e).

To miniaturize the magnetic active actuators and robots, a few studies have been conducted on fabricating magnetically-active 3D microstructures using direct and indirect 3D printing approaches [69,104,202–204]. Peters *et al.* [104] fabricated twist-type microrobots with programmed magnetic anisotropy using a 2PP process in Fig. 17(a), and their swimming properties in water were demonstrated under a rotating magnetic field. The direction in which the particles were aligned during fabrication by applying a magnetic field represented the easy magnetization axis, and enabled the devices to perform motion. Additionally, a surface functionalization on micro-swimmers was exploited by glycine grafting and subsequent immobilization of human immunoglobulin, providing a platform for biomedical applications. In the following, Peters *et al.* [205] successfully printed degradable superparamagnetic hydrogel microrobots by the same approach. The micro-swimmers enabled location based on corkscrew propulsion mechanism. Moreover, by dispersing magnetic particles into a polymer matrix, DIW methods were explored for printing magnetic devices. For example, Kim *et al.* [36] manufactured magnetic driving untethered small-scale robots using magnetic-assisted DIW. The orientation and location of the magnetic particles within the polymer can be controlled under the magnetic field, therefore, the printed structures can easily undergo complex locomotion as depicted in Fig. 17(b). Furthermore, magnetic actuation in Fig. 17(c) [206]. As depicted in Fig. 17(d), this soft continuum robot with hydrogel skin

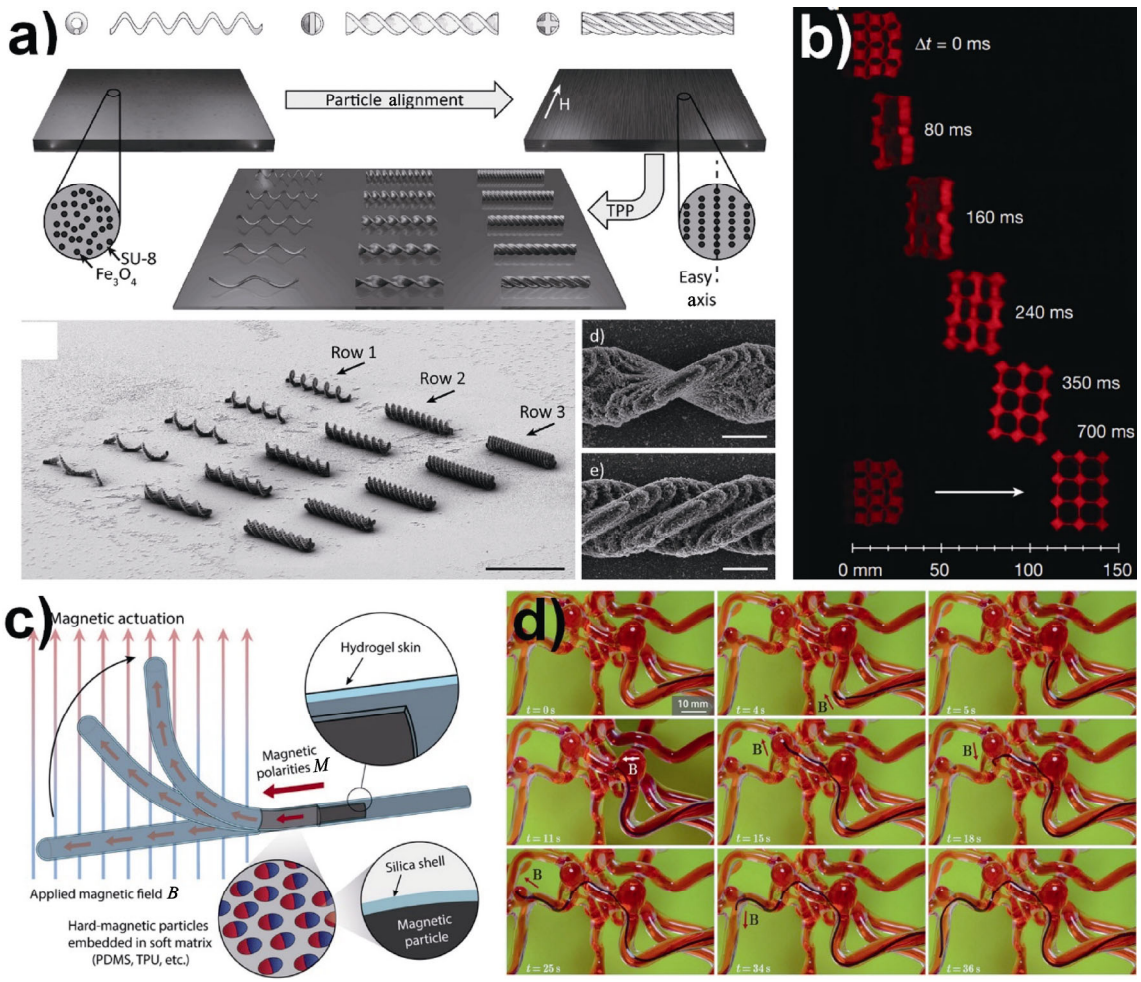

Fig. 17 (a) Fabrication of swimming microrobots with particle alignment and 2PP. Reproduced with permission from Ref. [104], © WILEY-VCH Verlag GmbH & Co. KGaA, Weinheim 2014. (b) Horizontal leap of a 3D auxetic structure. Reproduced with permission from Ref. [36], © Macmillan Publishers Ltd., part of Springer Nature 2018. (c) Schematic illustration of the magnetically responsive tip; (d) demonstration of navigating through a 3D cerebrovascular. Reproduced with permission from Ref. [206], © The American Association for the Advancement of Science 2019.

was able to smoothly navigate through constrained environments, such as a 3D cerebrovascular phantom using this method, they printed a submillimeter-scale soft robot capable of steering and navigating based on network, providing great potential in invasive surgery for inaccessible lesions. Coupling 3D printing to magnetism integration provides tremendous opportunities to manipulate and control soft robots and actuators suitable for extremely complex environments.

5. 2 Transformers

Magnetic materials have been viewed as ideal materials for use in electronics applications. Within 3D printing, electrical systems can be direct print into complex geometries difficult or impossible to achieve by other means, allowing customization for a specific end user application [207–209]. Inductors and transformers, crucial components for most electronics, have been widely investigated [78,210,211]. A fully integrated magnetic inductor was fabricated using extrusion-based 3D printing [210]. Magnetic and conductive pastes were deposited into 3D structures for power electronics circuits, followed by heating for curing polymers. The achieved magnetic relative permeability was 23.

To further improve the performance, there is an approach to incorporating magnetic materials into 3D-printed structures [211]. A microfluidic magnetic core inductor was fabricated by an SL 3D printer [212]. The systems were then filled with liquid metal and ferrofluid to create inductors, transformers, and wireless power coils as demonstrated in Fig. 18(a) [211]. Moreover, the possibility of producing a transformer core was also explored using FDM methods, due to the essential role in voltage conversion in power electronics [78]. The internal fill characteristics of printed transformer core were shown in Fig. 18(b). It was observed that the high fill factors can generate a more responsive transformer. Inkjet printing of electromagnetic responsive materials was also reported as presented in Fig. 18(c) [188]. The printed structures demonstrated high permittivity with tunable electromagnetic properties.

5. 3 Energy harvester

Recently, numerous studies have been focused on

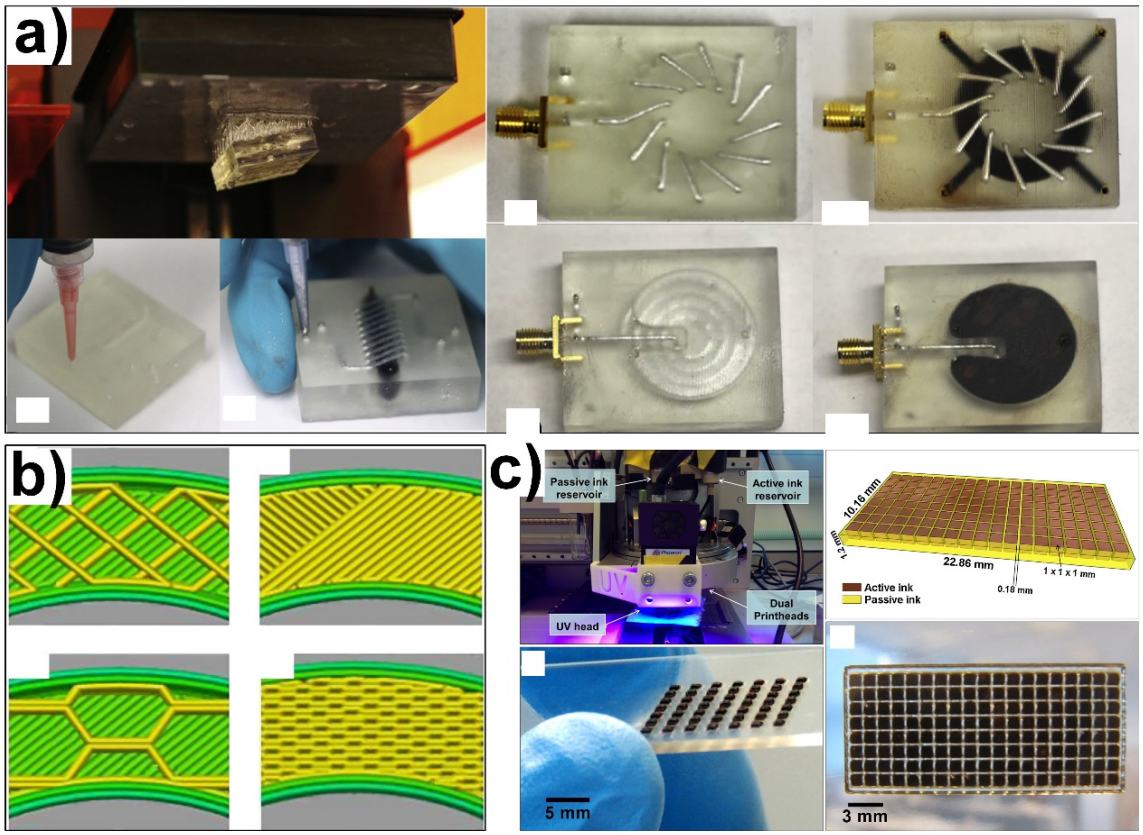

Fig. 18 (a) Ferrofluid-cored 3D-printed inductor. Reproduced with permission from Ref. [211], © Elsevier B.V. 2019. (b) Horizontal cross-sections of transformer cores. Reproduced with permission from Ref. [78], © Elsevier B.V. 2017. (c) Inkjet-printed waffle shape sample. Reproduced with permission from Ref. [188], © The Authors 2016.

energy conversion based on magnetic materials and composites [213–216]. Customized magnets with a high-energy product are required in the energy harvester. To avoid the complicated manufacturing process for the production of sintered magnets, 3D printing is extremely desired and suitable to reduce processing costs. Wang *et al.* [217] printed a magnet with the optimized topology using FDM process in Fig. 19(a). Compared to a non-optimized magnet, the optimized energy harvester provided an enhanced distortion power factor and high power density, demonstrating great potential for self-powered applications. At last, it is worth noting initial trials in combining distinct functionalities. Urbanek *et al.* [218] described the design and additively manufactured a soft magnetic rotor together with a shaft for a permanent magnet synchronous machine. To achieve electromagnetic requirements, ferromagnetic materials including ferro-silicon and ferro-cobalt alloys were additively processed with microstructures shown in Fig. 19(b). As discussed above, 3D printing can be applied to shape magnetic materials instead of conventional approaches, offering outstanding potentials for producing electronics in mass production.

5. 4 Electromagnetic microwave absorption

Nowadays, electromagnetic interference and electro magnetic pollution become serious since overexposure to electronic device could be harmful to humans. To solve the problems, microwave absorbers with the ability of absorbing unwanted electromagnetic signals have attracted considerable attention. Fortunately, soft ferrites with high complex permittivity and permeability are able to absorb electromagnetic waves. 3D printing of magnetic ferrites with intricate structures are therefore very attractive [177]. For example, Qian *et al.* [79] prepared magnetic composites by utilizing FDM technique with the addition of different contents $Li_{0.44}Zn_{0.2}Fe_{2.36}O_4$ (LZFO) particles into polymer matrix. The resulting microwave absorption property suggested that the maximum reflection loss values of 3D-printed

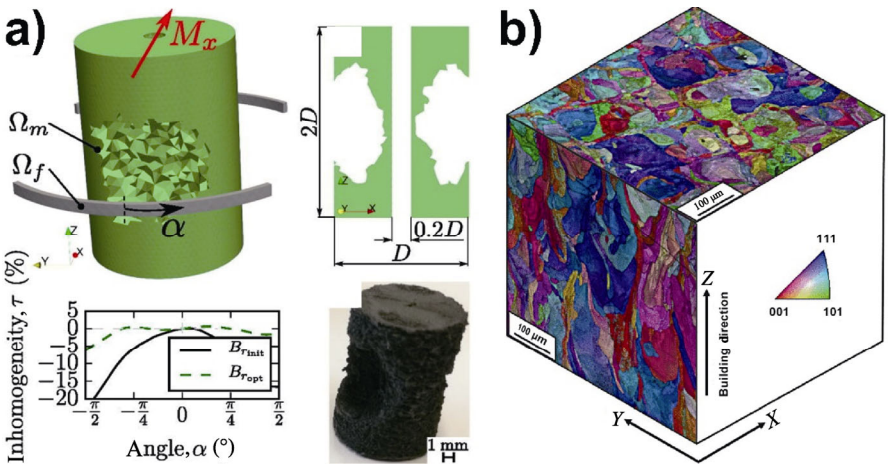

Fig. 19 (a) Topology optimized and 3D-printed magnet for the energy harvester. Reproduced with permission from Ref. [217], © Author(s) 2019. (b) The electron backscatter diffraction (EBSD) inverse pole figure map. Reproduced with permission from Ref. [218], © IEEE 2018.

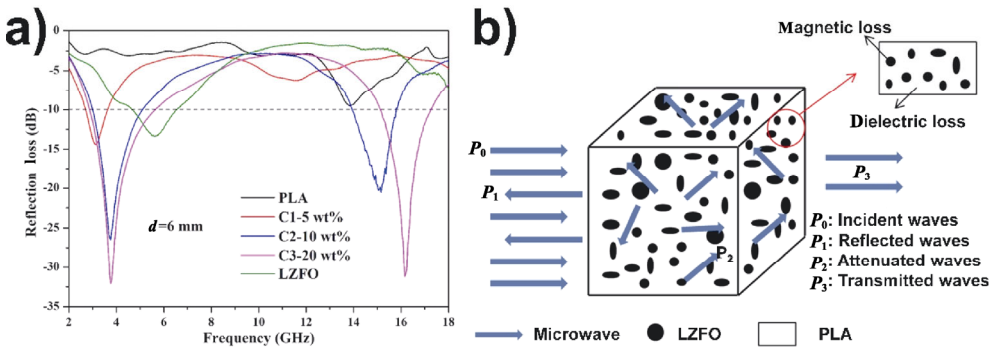

Fig. 20 (a) Reflection loss of 3D-printed samples with different $Li_{0.44}Zn_{0.2}Fe_{2.36}O_4$ contents; (b) schematic illustration of microwave absorption. Reproduced with permission from Ref. [79], © Springer Science Business Media, LLC, part of Springer Nature 2018.

composite could reach −32.4 dB at 3.8 GHz and −31.8 dB at 16.1 GHz as shown in Fig. 20(a) [79]. It is also worth to mention that the absorption properties significantly increased with the increase of the fraction of LZFO, which can be schematically illustrated in Fig. 20(b) [79]. More importantly, the 3D-printed microwave absorption materials with intricate shapes are promising alternatives to traditional-coated type absorbing materials. Therefore, 3D printing technology is able to fabricate magnetic materials with complex structures and excellent wave absorbing properties, which might become the developing trend in the future.

5. 5 Drug delivery

3D printing is a powerful tool to enable the production of biomedical devices with unprecedented complexity and functionality that would be challenging by traditional methods. Recently, 3D printing has found widespread applications in biomedical engineering, such as tissue scaffolding and drug delivery [46,47,77,92,219].

Integration of magnetic particles in materials could afford magnetism to the original materials [220–222]. Due to the remote wireless controllable property, magnetic actuation has attracted much research attention and used clinically for implantable biomedical devices. For example, Chin *et al.* [223] developed 3D-printed medical devices by incorporating superparamagnetic Fe_3O_4 nanoparticles into hydrogels as shown in Fig. 21(a). The magnetic materials allowed remote control, and complex structures with intricate and composite patterns in each layer were built in Fig. 21(b). It is worthwhile to mention that features in the manufactured biocompatible materials can down to micrometers in scale. Notably, magnetically-powered microrobots are promising for biomedical applications because they would not be ingested by tissues [204,224]. More impressively, aligned magnetic nanoparticles encapsulated by polymer matrix can be fabricated using a magnetic field assisted 3D printing process in Figs. 21(c) and 21(d) [225]. Compared to those with random particles, the printed aligning structures via magnetic control showed reinforced mechanical properties to maximize their performance. Moreover, the results also reported the suitability of this printed bioinspired array for drug delivery. Similarly, Xu *et al.* [77] demonstrated a targeted drug delivery system using a sperm-driven micromotor system as demonstrated in Fig. 21(e). The system was mainly composed of a magnetic tubular microstructure fabricated by means of two-photon 3D nanolithography. Subsequently, the microstructure was coated with magnetic iron nanoparticles for controllable magnetic guidance. Under guiding and release mechanisms, this micromotor can deliver drug to targeted tumor cells. Therefore, 3D printing can easily fabricate microstructures with complex geometries and potential biomedical performance. In addition, 3D printing has also been developed to fabricate biomedical scaffolds for bone tissue engineering [226,227].

Inspired by them, Zhang *et al.* [60] manufactured porous bioactive glass/polycaprolactone (Fe_3O_4/MBG/PCL) magnetic composite scaffolds using DIW. The scaffold demonstrated multifunctionality of bone regeneration, anticancer drug delivery, and magnetic hyperthermia. Moreover, Li *et al.* [49] also printed a polycaprolactone (PCL) scaffold, and decorated with hydrogel to improve the biocompatibility. With the addition of magnetic nanoparticles, the printed scaffold can be applied to construct biologically bile ducts. Although these examples are just tips of the iceberg, they indicate the possibility of 3D printing approaches for biomedical applications with remote magnetic actuation and control in enclosed and confined spaces.

5. 6 Magnetic separation

With the rapid growth of industrial and domestic activities, water pollution has evoked elevated worldwide concern as it leads to threatening diseases and disorders in living organisms. Hence, it is of utmost importance to purify water because it is one of the basic need for humans. Concerning this, various treatment techniques have been used for water remediation which could be from oil removal to oil/water separation to organic contaminant and heavy metal removal [228]. Specifically, magnetic materials with ferromagnetism and paramagnetism have shed light on this field [54]. For ferromagnetic materials, magnetism could be retained even after removal of the external magnetic field. For paramagnetic materials, however, the magnetic moment quickly drops to zero when the applied field is removed. It is fundamentally interesting to use magnetic materials for water remediation. Therefore, a plenty of research has been conducted on the purification of water using magnetic nanoparticles due to their high adsorption capacity and easy functionalization with various chemical groups [229–248]. The main principle is the adsorption followed by capturing and regenerating of magnetic powders. On this basis, magnetic separation has been developed to allow the gathering of materials using magnetic assistance several decades ago [249,250].

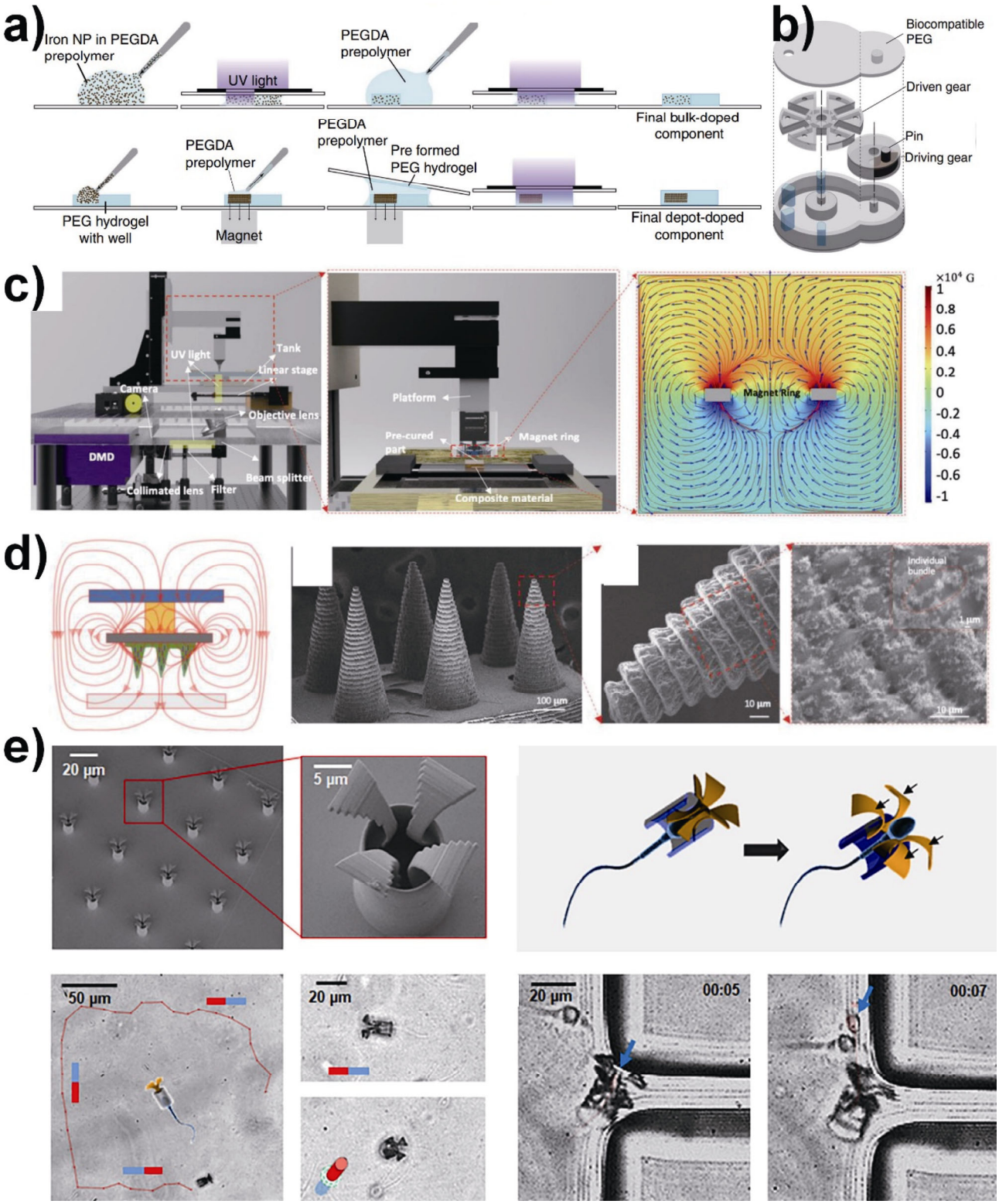

Fig. 21 (a) Two doping methods for incorporating iron oxide into components; (b) schematic diagram of an implantable hydrogel device. Reproduced with permission from Ref. [223], © The American Association for the Advancement of Science 2017. (c) Schematic diagram of the 3D printing process and simulation; (d) fabrication of limpet tooth-inspired array. Reproduced with permission from Ref. [225], © Wiley-VCH GmbH 2020. (e) Printed sperm-hybrid motor and release process. Reproduced with permission from Ref. [77], © American Chemical Society 2017.

More interestingly, a high gradient magnetic separation (HGMS) is a common technique for magnetic separation [251–256]. An HGMS system comprises of magnetically susceptible matrices installed inside an electromagnet, and magnetic matrices play an important role in the performance of the system. When an external field is applied, the matrices de-homogenize the magnetic field and generate high magnetic field gradients that attract magnetic particles and trap them there. Nonetheless, it was reported that magnetic nanoparticles held tightly on the metal matrices and were difficult to be recovered [257]. Thus, magnetic mesh structures with high magnetic susceptibility were 3D printed for effective magnetic separation of magnetic particles under a low magnetic field, and magnetic particles can be easily recovered as schematically illustrated in Fig. 22 [50]. In this work, $(Ni,Zn)Fe_2O_4$ was chosen due to its excellent magnetic properties, which can be magnetized under a relative low magnetic field. It should be noted that the multilayered mesh structure can be optimized by 3D printing, include diameter, distance, and number of layers, producing a high magnetic field gradient. Moreover, this mesh like a magnetic filter, is capable of capturing magnetic nanoparticles when the particles in the steam flow crosses the wires. The magnetic particles are subjected to a magnetic force (F_{mag}) as shown in Eq. (10):

$$F_{mag} = V_p M_p \nabla B \tag{10}$$

where V_p (m^3) is the particle volume, M_p (A/m) is the particle magnetization, and ∇B (T/m) is the gradient of magnetic flux density at the position of the particle. The competing forces in a magnetic separator include the hydrodynamic drag force (F_d) obtained from Stoke's equation in Eq. (11):

$$F_d = 6\pi\eta r_p \left(v_f - v_p\right) \tag{11}$$

where r_p (m) is the particle radius, and v_f and v_p (m/s) are the velocities of the fluid and particle, respectively. For successful collection of magnetic particles, the magnetic force attracting particles should override competing forces acting on the magnetic particles. Fortunately, it has been proved that magnetic particles were recovered and regenerated after the removal of magnetic field. In addition, the magnetic mesh can work well under harsh environment resulting from the intrinsic properties of ferrites ceramics with excellent chemical stability and mechanical hardness [258–261].

In some cases, magnetic hydrogel was used for efficient wastewater treatment when coupled with magnetic separation [262]. Notably, magnetic separation is commonly adopted for the purification of water. From

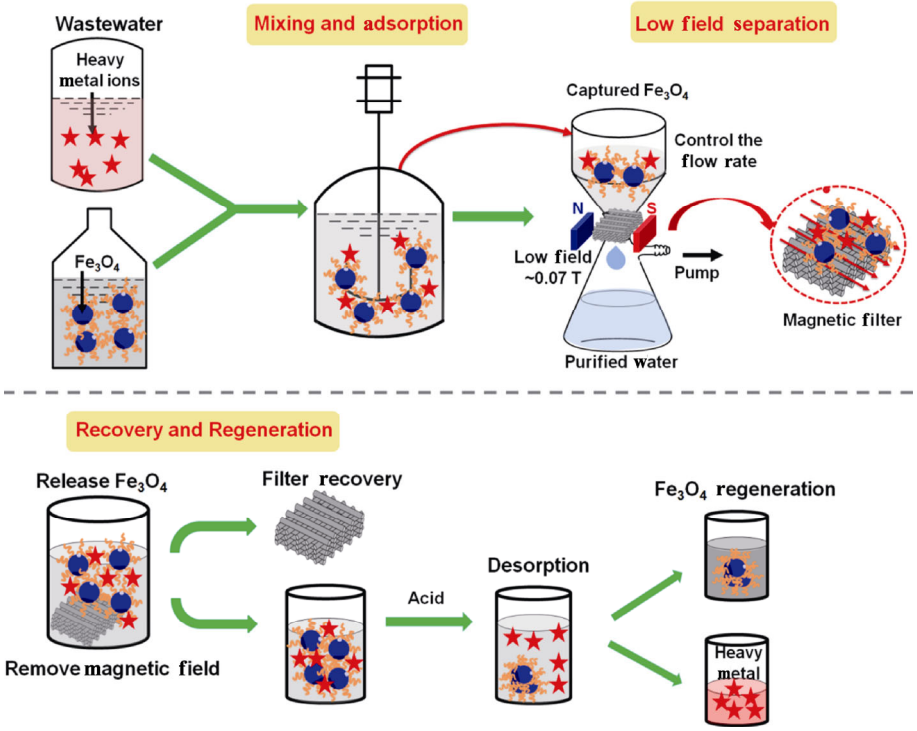

Fig. 22 Schematic illustration of low-field magnetic separation technique. Reproduced with permission from Ref. [50], © American Chemical Society 2017.

the point of view of recovery, magnetic separation system designs incorporating 3D printing of magnetic matrices would provide long term benefits. More interestingly, it is to be noted that electrospraying-based 3D printing has been utilized to form polyamide membrane [263]. The thickness and roughness of membrane can be controlled with high printing precision, resulting in a free-standing film that is smoother and thinner than traditional films. The adoption of 3D printing enables the development of separations for water remediation.

5. 7 Magnetic levitation

To date, most research has focused on ferromagnetic and paramagnetic materials, but diamagnetic materials also pave the way for many applications by magnetic manipulation. The fundamentals of magnetic propulsion were comprehensively reviewed in Refs. [88,264–266]. When diamagnetic object is placed in an external field, it can be levitated by repelling the applied magnetic field [267,268]. Actually, superconductors are perfect diamagnetic materials which expel the magnetic flux when cooled below the critical temperature. It is strongly believed that high-temperature superconductor is promising for application since it can be cooled down by liquid nitrogen [269,270].

To provide complex structures for wide applications, it is natural to come up with the idea of 3D printing since it offers specific design, on-demand fabrication, and high productivity [271]. Recently, YBCO ($YBa_2Cu_3O_{7-x}$) superconductor has been produced by extrusion-based 3D printing in our previous works [26,80]. In this work, the precursor powders were subjected to mechanical milling and subsequently dispersed in the organic solution for 3D printing. Finally, hollow structures which can store liquid nitrogen cryogenics were obtained with high critical current density and excellent superconducting properties as depicted in Fig. 23(a) [80]. It was obvious that large field can be trapped by decreasing the temperature. On the basis of superconducting properties, the printed hollow structures capable of storing liquid nitrogen stably levitated over a permanent magnet without any assistance as schematically shown in Fig. 23(b). The levitation time prolonged for more than 3 min, which was mainly attributed to the designed architectures, refined particles from milling technique, and optimized heat treatment. Interestingly, the printed sample also demonstrated the potential as a magnetic rotating bearing as indicated in Fig. 23(c). It was observed that a commercial permanent magnet could automatically levitate over the superconductor. Therefore, it is of great research significance to realize the practical magnetic levitation by 3D printing.

6 Challenges associated with 3D printing of magnetic materials

Although some interesting efforts have been observed, 3D printing of magnetic materials with high performance is still challenging to facilitate wide industrial applications:

1) Despite 3D printing with shape flexibility, it is necessary to explore geometries not feasible to be achieved by state-of-the-art methods, and have unique and potentially useful magnetic functionality. The next generation of 3D printing will enable not only the fabrication of multiple materials but also obtain multi-functionality with high resolution that was not possible previously.

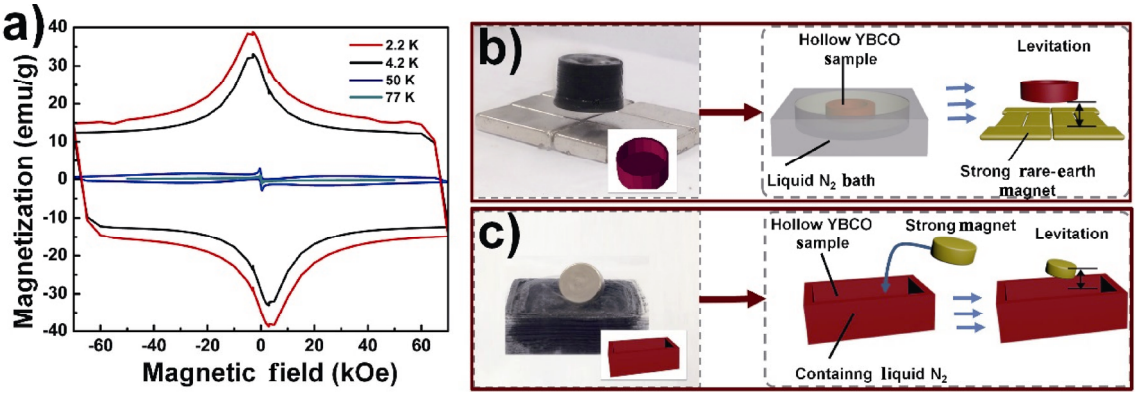

Fig. 23 (a) Magnetic hysteresis loops of YBCO; (b) levitation of the printed YBCO; (c) magnet levitated and rotated on top of the printed YBCO. Reproduced with permission from Ref. [80], © The Royal Society of Chemistry 2017.

2) For powder bed 3D printing, the powder properties should be optimized to improve flowability. During printing, the influence of microstructural and residual stress on magnetic properties needs to be exhaustively studied. For material extrusion approaches, such as FDM and DIW, it remains a challenge to produce magnetic materials with good surface finish and accuracy. Moreover, it is also difficult to precisely control the porosity, grain size, and desired magnetic properties in the printed magnets. Additionally, it is necessary to increase the volume fraction of magnetic fillers for performance enhancement. However, the homogeneous dispersion of magnetic fillers in polymer matrix is another challenge in 3D printing.

3) The functional magnetic properties are mainly determined by the microstructures developed during processing. The fabrication of full-dense high-energy magnetic materials with a desired microstructure is still a challenging task. Concerning ferrites, mechanical properties could hardly compete with traditional processing approaches for some specific applications. Moreover, it is worthwhile to mention that additional efforts for *in situ* magnetic field alignment of particles during printing need to be further implemented, as they could induce the desired anisotropic magnetic and mechanical properties.

4) As the abovementioned publications, researchers in different disciplines have explored some applications with 3D-printed magnets. To facilitate new applications, magnetic materials with locally oriented arrays and tailored magnetic properties are in highly demanding.

7 Conclusions

This paper focuses on reviewing previous studies related to the fabrication of magnetic materials using different 3D printing technologies for some special applications. 3D printing is capable of fabricating near-net-shape magnetic materials with the significant advantage of minimum rare-earth material waste and no tooling requirement. Many hard magnets, soft magnets, and composites have been successfully produced using various 3D printing approaches, in particular powder bed and material extrusion type processes. Choosing the appropriate method mainly depends on the design, starting materials, printer performance, and purposes. It is worthwhile noting that the magnetic properties of 3D-printed materials depend on structural design, raw materials selection, volumetric fraction of magnetic materials, and 3D printing processing. Additionally, 3D printing with the aid of magnetic field can construct high-performance anisotropic composites. Thanks to the functional magnetic properties, 3D-printed magnetic materials have found applications in many fields. Here, we focused more on the advances in soft robotics, transformers, microwave absorption, drug delivery, magnetic separation, and magnetic levitation. Consequently, the creation of magnetic materials with nearly any imaginable geometries can be made using CAD models to be fabricated by 3D printing. In the future, 3D printing of magnetic materials will lead to new avenues at this foundation.

Acknowledgements

This research work was financially supported by the Natural Science Foundation of Shandong Province (No. ZR2020QE040). Ming-Liang JIN would like to thank the financial support by the Young Taishan Scholars Program of Shandong Province (No. 201909099).

Declaration of competing interest

The authors have no competing interests to declare that are relevant to the content of this article.

References

[1] Gutfleisch O, Willard MA, Brück E, *et al.* Magnetic materials and devices for the 21st century: Stronger, lighter, and more energy efficient. *Adv Mater* 2011, **23**: 821–842.

[2] Zhao WL, Lipo TA, Kwon BI. Comparative study on novel dual stator radial flux and axial flux permanent magnet motors with ferrite magnets for traction application. *IEEE Trans Magn* 2014, **50**: 8104404.

[3] Jang SM, Seo HJ, Park YS, *et al.* Design and electromagnetic field characteristic analysis of 1.5 kW small scale wind power generator for substitution of Nd–Fe–B to ferrite permanent magnet. *IEEE Trans Magn* 2012, **48**: 2933–2936.

[4] Jian G, Zhou DX, Yang JY, *et al.* Tape casting of cobalt ferrite from nonaqueous slurry. *J Magn Magn Mater* 2012, **324**: 4179–4183.

[5] Jantunen H, Hu T, Uusimäki A, *et al.* Tape casting of ferroelectric, dielectric, piezoelectric and ferromagnetic materials. *J Eur Ceram Soc* 2004, **24**: 1077–1081.

[6] Tseng TY, Lin JC. Microstructure and properties of Ni–Zn ferrites sintered from slip cast colloidally precipitated particles. *IEEE Trans Magn* 1989, **25**: 4405–4408.

[7] Murillo N, González J, Guraya C, *et al.* Structural and magnetic properties of sintered Sr-ferrites fabricated by powder injection molding. *J Magn Magn Mater* 1999, **203**: 165–168.

[8] Ye Y, Qiao L, Zheng JW, *et al.* Effect of microcrystalline wax on the solvent debinding of the Sr-ferrite ceramics prepared by powder injection molding. *J Eur Ceram Soc* 2017, **37**: 2105–2114.

[9] Gutiérrez-López J, Rodriguez-Senín E, Pastor JY, *et al.* Microstructure, magnetic and mechanical properties of Ni–Zn ferrites prepared by powder injection moulding. *Powder Technol* 2011, **210**: 29–35.

[10] Saura-Múzquiz M, Granados-Miralles C, Stingaciu M, *et al.* Improved performance of $SrFe_{12}O_{19}$ bulk magnets through bottom-up nanostructuring. *Nanoscale* 2016, **8**: 2857–2866.

[11] Stingaciu M, Topole M, McGuiness P, *et al.* Magnetic properties of ball-milled $SrFe_{12}O_{19}$ particles consolidated by spark-plasma sintering. *Sci Rep* 2015, **5**: 14112.

[12] Eikeland AZ, Stingaciu M, Granados-Miralles C, *et al.* Enhancement of magnetic properties by spark plasma sintering of hydrothermally synthesised $SrFe_{12}O_{19}$. *CrystEngComm* 2017, **19**: 1400–1407.

[13] Bollero A, Rial J, Villanueva M, *et al.* Recycling of strontium ferrite waste in a permanent magnet manufacturing plant. *ACS Sustain Chem Eng* 2017, **5**: 3243–3249.

[14] Stansbury JW, Idacavage MJ. 3D printing with polymers: Challenges among expanding options and opportunities. *Dent Mater* 2016, **32**: 54–64.

[15] Yuk HW, Lu BY, Lin S, *et al.* 3D printing of conducting polymers. *Nat Commun* 2020, **11**: 1604.

[16] Su XR, Li XW, Ong CYA, *et al.* Metallization of 3D printed polymers and their application as a fully functional water-splitting system. *Adv Sci*: *Weinh* 2019, **6**: 1801670.

[17] Mao YQ, Yu K, Isakov MS, *et al.* Sequential self-folding structures by 3D printed digital shape memory polymers. *Sci Rep* 2015, **5**: 13616.

[18] Yamada A, Niikura F, Ikuta K. A three-dimensional microfabrication system for biodegradable polymers with high resolution and biocompatibility. *J Micromech Microeng* 2008, **18**: 025035.

[19] Huang XL, Chang S, Lee WSV, *et al.* Three-dimensional printed cellular stainless steel as a high-activity catalytic electrode for oxygen evolution. *J Mater Chem A* 2017, **5**: 18176–18182.

[20] Xie FX, He XB, Cao SL, *et al.* Structural and mechanical characteristics of porous 316L stainless steel fabricated by indirect selective laser sintering. *J Mater Process Technol* 2013, **213**: 838–843.

[21] Jakus AE, Taylor SL, Geisendorfer NR, *et al.* Metallic architectures from 3D-printed powder-based liquid inks. *Adv Funct Mater* 2015, **25**: 6985–6995.

[22] Noguera R, Lejeune M, Chartier T. 3D fine scale ceramic components formed by ink-jet prototyping process. *J Eur Ceram Soc* 2005, **25**: 2055–2059.

[23] Chen ZW, Li ZY, Li JJ, *et al.* 3D printing of ceramics: A review. *J Eur Ceram Soc* 2019, **39**: 661–687.

[24] Cheng J, Chen Y, Wu JW, *et al.* 3D printing of $BaTiO_3$ piezoelectric ceramics for a focused ultrasonic array. *Sensors* 2019, **19**: 4078.

[25] Wei XX, Liu YH, Zhao DJ, *et al.* 3D printing of piezoelectric barium titanate with high density from milled powders. *J Eur Ceram Soc* 2020, **40**: 5423–5430.

[26] Wei XX, Nagarajan RS, Peng E, *et al.* Fabrication of $YBa_2Cu_3O_{7-x}$ (YBCO) superconductor bulk structures by extrusion freeforming. *Ceram Int* 2016, **42**: 15836–15842.

[27] Peng E, Wei XX, Garbe U, *et al.* Robocasting of dense yttria-stabilized zirconia structures. *J Mater Sci* 2018, **53**: 247–273.

[28] Lakhdar Y, Tuck C, Binner J, *et al.* Additive manufacturing of advanced ceramic materials. *Prog Mater Sci* 2021, **116**: 100736.

[29] He RJ, Zhou NP, Zhang KQ, *et al.* Progress and challenges towards additive manufacturing of SiC ceramic. *J Adv Ceram* 2021, **10**: 637–674.

[30] Farahani RD, Dubé M, Therriault D. Three-dimensional printing of multifunctional nanocomposites: Manufacturing techniques and applications. *Adv Mater* 2016, **28**: 5794–5821.

[31] Valino AD, Dizon JRC, Espera Jr AH, *et al.* Advances in 3D printing of thermoplastic polymer composites and nanocomposites. *Prog Polym Sci* 2019, **98**: 101162.

[32] Wang X, Jiang M, Zhou ZW, *et al.* 3D printing of polymer matrix composites: A review and prospective. *Compos B Eng* 2017, **110**: 442–458.

[33] Kim K, Zhu W, Qu X, *et al.* 3D optical printing of piezoelectric nanoparticle-polymer composite materials. *ACS Nano* 2014, **8**: 9799–9806.

[34] Dermanaki Farahani R, Dubé M. Printing polymer nanocomposites and composites in three dimensions. *Adv Eng Mater* 2018, **20**: 1700539.

[35] Zhang X, Yao JH, Liu B, *et al.* Three-dimensional high-entropy alloy-polymer composite nanolattices that overcome the strength-recoverability trade-off. *Nano Lett* 2018, **18**: 4247–4256.

[36] Kim Y, Yuk H, Zhao R, *et al.* Printing ferromagnetic domains for untethered fast-transforming soft materials. *Nature* 2018, **558**: 274–279.

[37] Guo SZ, Qiu KY, Meng FB, *et al.* 3D printed stretchable tactile sensors. *Adv Mater* 2017, **29**: 1701218.

[38] Zhao JX, Zhang Y, Huang YN, *et al.* 3D printing fiber electrodes for an all-fiber integrated electronic device via hybridization of an asymmetric supercapacitor and a temperature sensor. *Adv Sci*: *Weinh* 2018, **5**: 1801114.

[39] Sun K, Wei TS, Ahn BY, *et al.* 3D printing of interdigitated Li-ion microbattery architectures. *Adv Mater* 2013, **25**: 4539–4543.

[40] McOwen DW, Xu SM, Gong YH, *et al.* 3D-printing electrolytes for solid-state batteries. *Adv Mater* 2018, **30**: 1707132.

[41] Park J, Kim JK, Kim DS, *et al.* Wireless pressure sensor

integrated with a 3D printed polymer stent for smart health monitoring. *Sens Actuat B Chem* 2019, **280**: 201–209.

[42] Gul JZ, Sajid M, Rehman MM, *et al.* 3D printing for soft robotics—A review. *Sci Technol Adv Mater* 2018, **19**: 243–262.

[43] Bartlett NW, Tolley MT, Overvelde JTB, *et al.* A 3D-printed, functionally graded soft robot powered by combustion. *Science* 2015, **349**: 161–165.

[44] Wallin TJ, Pikul J, Shepherd RF. 3D printing of soft robotic systems. *Nat Rev Mater* 2018, **3**: 84–100.

[45] Neufurth M, Wang XH, Wang SF, *et al.* 3D printing of hybrid biomaterials for bone tissue engineering: Calcium-polyphosphate microparticles encapsulated by polycaprolactone. *Acta Biomater* 2017, **64**: 377–388.

[46] Melchels FPW, Feijen J, Grijpma DW. A review on stereolithography and its applications in biomedical engineering. *Biomaterials* 2010, **31**: 6121–6130.

[47] Hwang HH, Zhu W, Victorine G, *et al.* 3D-printing of functional biomedical microdevices via light- and extrusion-based approaches. *Small Methods* 2018, **2**: 1700277.

[48] Beg S, Almalki WH, Malik A, *et al.* 3D printing for drug delivery and biomedical applications. *Drug Discov Today* 2020, **25**: 1668–1681.

[49] Li HH, Yin YX, Xiang Y, *et al.* A novel 3D printing PCL/GelMA scaffold containing USPIO for MRI-guided bile duct repair. *Biomed Mater* 2020, **15**: 045004.

[50] Wei XX, Sugumaran PJ, Peng E, *et al.* Low-field dynamic magnetic separation by self-fabricated magnetic meshes for efficient heavy metal removal. *ACS Appl Mater Interfaces* 2017, **9**: 36772–36782.

[51] Tian XC, Jin J, Yuan SQ, *et al.* Emerging 3D-printed electrochemical energy storage devices: A critical review. *Adv Energy Mater* 2017, **7**: 1700127.

[52] Qiao HY, Zhang Y, Huang ZG, *et al.* 3D printing individualized triboelectric nanogenerator with macro-pattern. *Nano Energy* 2018, **50**: 126–132.

[53] Li R, Yuan SQ, Zhang W, *et al.* 3D printing of mixed matrix films based on metal-organic frameworks and thermoplastic polyamide 12 by selective laser sintering for water applications. *ACS Appl Mater Interfaces* 2019, **11**: 40564–40574.

[54] Du R, Zhao QC, Zheng Z, *et al.* 3D self-supporting porous magnetic assemblies for water remediation and beyond. *Adv Energy Mater* 2016, **6**: 1600473.

[55] Ruiz-Morales JC, Tarancón A, Canales-Vázquez J, *et al.* Three dimensional printing of components and functional devices for energy and environmental applications. *Energy Environ Sci* 2017, **10**: 846–859.

[56] Lantean S, Barrera G, Pirri CF, *et al.* 3D printing of magnetoresponsive polymeric materials with tunable mechanical and magnetic properties by digital light processing. *Adv Mater Technol* 2019, **4**: 1900505.

[57] Huber C, Abert C, Bruckner F, *et al.* 3D print of polymer bonded rare-earth magnets, and 3D magnetic field scanning with an end-user 3D printer. *Appl Phys Lett* 2016, **109**: 162401.

[58] Yang F, Zhang XY, Guo ZM, *et al.* 3D printing of NdFeB bonded magnets with $SrFe_{12}O_{19}$ addition. *J Alloys Compd* 2019, **779**: 900–907.

[59] Sonnleitner K, Huber C, Teliban I, *et al.* 3D printing of polymer-bonded anisotropic magnets in an external magnetic field and by a modified production process. *Appl Phys Lett* 2020, **116**: 092403.

[60] Zhang JH, Zhao SC, Zhu M, *et al.* 3D-printed magnetic Fe_3O_4/MBG/PCL composite scaffolds with multifunctionality of bone regeneration, local anticancer drug delivery and hyperthermia. *J Mater Chem B* 2014, **2**: 7583–7595.

[61] Domingo-Roca R, Jackson JC, Windmill JFC. 3D-printing polymer-based permanent magnets. *Mater Des* 2018, **153**: 120–128.

[62] Zhu PF, Yang WY, Wang R, *et al.* 4D printing of complex structures with a fast response time to magnetic stimulus. *ACS Appl Mater Interfaces* 2018, **10**: 36435–36442.

[63] Li L, Tirado A, Nlebedim IC, *et al.* Big area additive manufacturing of high performance bonded NdFeB magnets. *Sci Rep* 2016, **6**: 36212.

[64] Paranthaman MP, Shafer CS, Elliott AM, *et al.* Binder jetting: A novel NdFeB bonded magnet fabrication process. *JOM* 2016, **68**: 1978–1982.

[65] Martin JJ, Fiore BE, Erb RM. Designing bioinspired composite reinforcement architectures via 3D magnetic printing. *Nat Commun* 2015, **6**: 8641.

[66] Martin JJ, Caunter A, Dendulk A, *et al.* Direct-write 3D printing of composite materials with magnetically aligned discontinuous reinforcement. In: Proceedings of the Proc SPIE 10194, Micro- and Nanotechnology Sensors, Systems, and Applications IX, Anaheim, USA, 2017, **10194**: 258–271.

[67] Bastola AK, Paudel M, Li L. Dot-patterned hybrid magnetorheological elastomer developed by 3D printing. *J Magn Magn Mater* 2020, **494**: 165825.

[68] Wei XX, Liu YH, Zhao DJ, *et al.* Net-shaped barium and strontium ferrites by 3D printing with enhanced magnetic performance from milled powders. *J Magn Magn Mater* 2020, **493**: 165664.

[69] Shao GB, Ware HOT, Li LQ, *et al.* Rapid 3D printing magnetically active microstructures with high solid loading. *Adv Eng Mater* 2020, **22**: 1900911.

[70] Hodaei A, Akhlaghi O, Khani N, *et al.* Single additive enables 3D printing of highly loaded iron oxide suspensions. *ACS Appl Mater Interfaces* 2018, **10**: 9873–9881.

[71] Hassan RU, Jo SW, Seok JW. Fabrication of a functionally graded and magnetically responsive shape memory polymer using a 3D printing technique and its characterization. *J Appl Polym Sci* 2018, **135**: 45997.

[72] Popov V, Koptyug A, Radulov I, *et al.* Prospects of additive manufacturing of rare-earth and non-rare-earth permanent magnets. *Procedia Manuf* 2018, **21**: 100–108.

[73] Li L, Post B, Kunc V, *et al.* Additive manufacturing of near-net-shape bonded magnets: Prospects and challenges. *Scripta Mater* 2017, **135**: 100–104.

[74] Périgo EA, Jacimovic J, García Ferré F, *et al.* Additive manufacturing of magnetic materials. *Addit Manuf* 2019, **30**: 100870.

[75] Chaudhary V, Mantri SA, Ramanujan RV, *et al.* Additive manufacturing of magnetic materials. *Prog Mater Sci* 2020, **114**: 100688.

[76] Zhang CQ, Li XJ, Jiang LM, *et al.* 3D printing of functional magnetic materials: From design to applications. *Adv Funct Mater* 2021, **31**: 2102777.

[77] Xu HF, Medina-Sánchez M, Magdanz V, *et al.* Sperm-hybrid micromotor for targeted drug delivery. *ACS Nano* 2018, **12**: 327–337.

[78] Bollig LM, Hilpisch PJ, Mowry GS, *et al.* 3D printed magnetic polymer composite transformers. *J Magn Magn Mater* 2017, **442**: 97–101.

[79] Qian Y, Yao ZJ, Lin HY, *et al.* Mechanical and microwave absorption properties of 3D-printed $Li_{0.44}Zn_{0.2}Fe_{2.36}O_4$/polylactic acid composites using fused deposition modeling. *J Mater Sci Mater Electron* 2018, **29**: 19296–19307.

[80] Wei XX, Peng E, Xie YY, *et al.* Extrusion printing of a designed three-dimensional $YBa_2Cu_3O_{7-x}$ superconductor with milled precursor powder. *J Mater Chem C* 2017, **5**: 3382–3389.

[81] Coey JMD. Hard magnetic materials: A perspective. *IEEE Trans Magn* 2011, **47**: 4671–4681.

[82] Rezlescu L, Rezlescu E, Popa PD, *et al.* Fine barium hexaferrite powder prepared by the crystallisation of glass. *J Magn Magn Mater* 1999, **193**: 288–290.

[83] Brown DN. Fabrication, processing technologies, and new advances for RE–Fe–B magnets. *IEEE Trans Magn* 2016, **52**: 2101209.

[84] Gutfleisch O. Controlling the properties of high energy density permanent magnetic materials by different processing routes. *J Phys D*: *Appl Phys* 2000, **33**: R157–R172.

[85] Kneller EF, Hawig R. The exchange-spring magnet: A new material principle for permanent magnets. *IEEE Trans Magn* 1991, **27**: 3588–3560.

[86] Périgo EA, Weidenfeller B, Kollár P, *et al.* Past, present, and future of soft magnetic composites. *Appl Phys Rev* 2018, **5**: 031301.

[87] Coey JMD. Magnetic materials. *J Alloys Compd* 2001, **326**: 2–6.

[88] Rikken RS, Nolte RJ, Maan JC, *et al.* Manipulation of micro- and nanostructure motion with magnetic fields. *Soft Matter* 2014, **10**: 1295–1308.

[89] Coey JMD. Perspective and prospects for rare earth permanent magnets. *Engineering* 2020, **6**: 119–131.

[90] Utela B, Storti D, Anderson R, *et al.* A review of process development steps for new material systems in three dimensional printing (3DP). *J Manuf Process* 2008, **10**: 96–104.

[91] Duoss EB, Weisgraber TH, Hearon K, *et al.* Three-dimensional printing of elastomeric, cellular architectures with negative stiffness. *Adv Funct Mater* 2014, **24**: 4905–4913.

[92] Gross BC, Erkal JL, Lockwood SY, *et al.* Evaluation of 3D printing and its potential impact on biotechnology and the chemical sciences. *Anal Chem* 2014, **86**: 3240–3253.

[93] Kodama H. Automatic method for fabricating a three-dimensional plastic model with photo-hardening polymer. *Rev Sci Instrum* 1981, **52**: 1770–1773.

[94] Hull CW. Apparatus for production of three-dimensional objects by stereolithography. U.S. Patent 4 575 330, 1986.

[95] Lu Y, Mapili G, Suhali G, *et al.* A digital micro-mirror device-based system for the microfabrication of complex, spatially patterned tissue engineering scaffolds. *J Biomed Mater Res A* 2006, **77A**: 396–405.

[96] Sun C, Fang N, Wu DM, *et al.* Projection micro-stereolithography using digital micro-mirror dynamic mask. *Sens Actuat A Phys* 2005, **121**: 113–120.

[97] Tumbleston JR, Shirvanyants D, Ermoshkin N, *et al.* Continuous liquid interface production of 3D objects. *Science* 2015, **347**: 1349–1352.

[98] Cumpston BH, Ananthavel SP, Barlow S, *et al.* Two-photon polymerization initiators for three-dimensional optical data storage and microfabrication. *Nature* 1999, **398**: 51–54.

[99] Kuebler SM, Braun KL, Zhou WH, *et al.* Design and application of high-sensitivity two-photon initiators for three-dimensional microfabrication. *J Photochem Photobiol A Chem* 2003, **158**: 163–170.

[100] Rasaki SA, Xiong DY, Xiong SF, *et al.* Photopolymerization-based additive manufacturing of ceramics: A systematic review. *J Adv Ceram* 2021, **10**: 442–471.

[101] Zheng XY, Deotte J, Alonso MP, *et al.* Design and optimization of a light-emitting diode projection micro-stereolithography three-dimensional manufacturing system. *Rev Sci Instrum* 2012, **83**: 125001.

[102] Lu L, Guo P, Pan YY. Magnetic-field-assisted projection stereolithography for three-dimensional printing of smart structures. *J Manuf Sci Eng* 2017, **139**: 071008.

[103] Ji ZY, Yan CY, Yu B, *et al.* Multimaterials 3D printing for free assembly manufacturing of magnetic driving soft actuator. *Adv Mater Interfaces* 2017, **4**: 1700629.

[104] Peters C, Ergeneman O, García PDW, *et al.* Superparamagnetic twist-type actuators with shape-independent magnetic properties and surface functionalization for advanced biomedical applications. *Adv Funct Mater* 2014, **24**: 5269–5276.

[105] Baldissera AB, Pavez P, Wendhausen PAP, *et al.* Additive manufacturing of bonded Nd–Fe–B—Effect of process parameters on magnetic properties. *IEEE Trans Magn* 2017, **53**: 2101704.

[106] Jaćimović J, Binda F, Herrmann LG, *et al.* Net shape 3D printed NdFeB permanent magnet. *Adv Eng Mater* 2017, **19**: 1700098.

[107] Mikler CV, Chaudhary V, Borkar T, *et al.* Laser additive processing of Ni–Fe–V and Ni–Fe–Mo permalloys: Microstructure and magnetic properties. *Mater Lett* 2017, **192**: 9–11.

[108] Kumar S. Selective laser sintering: A qualitative and objective approach. *JOM* 2003, **55**: 43–47.

[109] Williams JM, Adewunmi A, Schek RM, *et al.* Bone tissue engineering using polycaprolactone scaffolds fabricated via selective laser sintering. *Biomaterials* 2005, **26**: 4817–4827.
[110] Huber C, Sepehri-Amin H, Goertler M, *et al.* Coercivity enhancement of selective laser sintered NdFeB magnets by grain boundary infiltration. *Acta Mater* 2019, **172**: 66–71.
[111] Kruth JP, Froyen L, Vaerenbergh JV, *et al.* Selective laser melting of iron-based powder. *J Mater Process Technol* 2004, **149**: 616–622.
[112] Prashanth KG, Eckert J. Formation of metastable cellular microstructures in selective laser melted alloys. *J Alloys Compd* 2017, **707**: 27–34.
[113] Jung HY, Choi SJ, Prashanth KG, *et al.* Fabrication of Fe-based bulk metallic glass by selective laser melting: A parameter study. *Mater Des* 2015, **86**: 703–708.
[114] Miao XF, Wang WY, Liang HX, *et al.* Printing $(Mn,Fe)_2(P,Si)$ magnetocaloric alloys for magnetic refrigeration applications. *J Mater Sci* 2020, **55**: 6660–6668.
[115] Goll D, Schuller D, Martinek G, *et al.* Additive manufacturing of soft magnetic materials and components. *Addit Manuf* 2019, **27**: 428–439.
[116] Goll D, Vogelgsang D, Pflanz U, *et al.* Refining the microstructure of Fe–Nd–B by selective laser melting. *Phys Status Solidi RRL Rapid Res Lett* 2019, **13**: 1800536.
[117] Heer B, Bandyopadhyay A. Compositionally graded magnetic-nonmagnetic bimetallic structure using laser engineered net shaping. *Mater Lett* 2018, **216**: 16–19.
[118] Lewis JA, Gratson GM. Direct writing in three dimensions. *Mater Today* 2004, **7**: 32–39.
[119] Palmero EM, Casaleiz D, Jiménez NA, *et al.* Magnetic-polymer composites for bonding and 3D printing of permanent magnets. *IEEE Trans Magn* 2019, **55**: 2101004.
[120] Patton MV, Ryan P, Calascione T, *et al.* Manipulating magnetic anisotropy in fused filament fabricated parts via macroscopic shape, mesoscopic infill orientation, and infill percentage. *Addit Manuf* 2019, **27**: 482–488.
[121] Huber C, Goertler M, Abert C, *et al.* Additive manufactured and topology optimized passive shimming elements for permanent magnetic systems. *Sci Rep* 2018, **8**: 14651.
[122] Smay JE, Cesarano J, Lewis JA. Colloidal inks for directed assembly of 3-D periodic structures. *Langmuir* 2002, **18**: 5429–5437.
[123] Compton BG, Lewis JA. 3D-printing of lightweight cellular composites. *Adv Mater* 2014, **26**: 5930–5935.
[124] Lewis JA. Direct ink writing of 3D functional materials. *Adv Funct Mater* 2006, **16**: 2193–2204.
[125] Smay JE, Gratson GM, Shepherd RF, *et al.* Directed colloidal assembly of 3D periodic structures. *Adv Mater* 2002, **14**: 1279–1283.
[126] Yang LL, Zeng XJ, Ditta A, *et al.* Preliminary 3D printing of large inclined-shaped alumina ceramic parts by direct ink writing. *J Adv Ceram* 2020, **9**: 312–319.
[127] Herschel WH, Bulkley R. Konsistenzmessungen von gummi-benzollösungen. *Kolloid-Zeitschrift* 1926, **39**: 291–300.
[128] Reed JS. *Introduction to the Principles of Ceramic Processing*. New York: Wiley, 1988.
[129] Janna WS. *Introduction to Fluid Mechanics*, 4th edn. Boston, USA: CRC Press, 2010.
[130] M'Barki A, Bocquet L, Stevenson A. Linking rheology and printability for dense and strong ceramics by direct ink writing. *Sci Rep* 2017, **7**: 6017.
[131] Faes M, Valkenaers H, Vogeler F, *et al.* Extrusion-based 3D printing of ceramic components. *Procedia CIRP* 2015, **28**: 76–81.
[132] Benbow JJ, Oxley EW, Bridgwater J. The extrusion mechanics of pastes—The influence of paste formulation on extrusion parameters. *Chem Eng Sci* 1987, **42**: 2151–2162.
[133] Benbow JJ. *Paste Flow and Extrusion*. Oxford, UK: Oxford University Press, 1993.
[134] Kokkinis D, Schaffner M, Studart AR. Multimaterial magnetically assisted 3D printing of composite materials. *Nat Commun* 2015, **6**: 8643.
[135] Khazdozian HA, Li L, Paranthaman MP, *et al.* Low-field alignment of anisotropic bonded magnets for additive manufacturing of permanent magnet motors. *JOM* 2019, **71**: 626–632.
[136] Erb RM, Libanori R, Rothfuchs N, *et al.* Composites reinforced in three dimensions by using low magnetic fields. *Science* 2012, **335**: 199–204.
[137] Erb RM, Cherenack KH, Stahel RE, *et al.* Locally reinforced polymer-based composites for elastic electronics. *ACS Appl Mater Interfaces* 2012, **4**: 2860–2864.
[138] Lu L, Baynojir Joyee E, Pan YY. Correlation between microscale magnetic particle distribution and magnetic-field-responsive performance of three-dimensional printed composites. *J Micro Nano Manuf* 2018, **6**: 010904.
[139] Joyee EB, Pan YY. Multi-material additive manufacturing of functional soft robot. *Procedia Manuf* 2019, **34**: 566–573.
[140] Tsumori F, Kawanishi H, Kudo K, *et al.* Development of three-dimensional printing system for magnetic elastomer with control of magnetic anisotropy in the structure. *Jpn J Appl Phys* 2016, **55**: 06GP18.
[141] Song H, Spencer J, Jander A, *et al.* Inkjet printing of magnetic materials with aligned anisotropy. *J Appl Phys* 2014, **115**: 17E308.
[142] Huber C, Mitteramskogler G, Goertler M, *et al.* Additive manufactured polymer-bonded isotropic NdFeB magnets by stereolithography and their comparison to fused filament fabricated and selective laser sintered magnets. *Materials* 2020, **13**: 1916.
[143] Nagarajan B, Eufracio Aguilera AF, Wiechmann M, *et al.* Characterization of magnetic particle alignment in photosensitive polymer resin: A preliminary study for additive manufacturing processes. *Addit Manuf* 2018, **22**: 528–536.
[144] Zhang BC, Fenineche NE, Zhu L, *et al.* Studies of magnetic properties of permalloy (Fe–30%Ni) prepared by SLM

technology. *J Magn Magn Mater* 2012, **324**: 495–500.
[145] Garibaldi M, Ashcroft I, Simonelli M, *et al.* Metallurgy of high-silicon steel parts produced using selective laser melting. *Acta Mater* 2016, **110**: 207–216.
[146] Li L, Tirado A, Conner BS, *et al.* A novel method combining additive manufacturing and alloy infiltration for NdFeB bonded magnet fabrication. *J Magn Magn Mater* 2017, **438**: 163–167.
[147] Li L, Jones K, Sales B, *et al.* Fabrication of highly dense isotropic Nd–Fe–B nylon bonded magnets via extrusion-based additive manufacturing. *Addit Manuf* 2018, **21**: 495–500.
[148] Hanemann T, Syperek D, Nötzel D. 3D printing of ABS Barium ferrite composites. *Materials* 2020, **13**: 1481.
[149] Khazdozian HA, Manzano JS, Gandha K, *et al*. Recycled Sm-Co bonded magnet filaments for 3D printing of magnets. *AIP Adv* 2018, **8**: 056722.
[150] Huber C, Cano S, Teliban I, *et al.* Polymer-bonded anisotropic $SrFe_{12}O_{19}$ filaments for fused filament fabrication. *J Appl Phys* 2020, **127**: 063904.
[151] [Compton BG, Kemp JW, Novikov TV, *et al.* Direct-write 3D printing of NdFeB bonded magnets. *Mater Manuf Process* 2018, **33**: 109–113.
[152] Peng E, Wei XX, Herng TS, *et al.* Ferrite-based soft and hard magnetic structures by extrusion free-forming. *RSC Adv* 2017, **7**: 27128–27138.
[153] Yang F, Zhang XY, Guo ZM, *et al.* 3D gel-printing of Sr ferrite parts. *Ceram Int* 2018, **44**: 22370–22377.
[154] Zhai FQ, Sun AZ, Yuan D, *et al.* Epoxy resin effect on anisotropic Nd–Fe–B rubber-bonded magnets performance. *J Alloys Compd* 2011, **509**: 687–690.
[155] Ormerod J, Constantinides S. Bonded permanent magnets: Current status and future opportunities (invited). *J Appl Phys* 1997, **81**: 4816–4820.
[156] Shen AL, Bailey CP, Ma AWK, *et al.* UV-assisted direct write of polymer-bonded magnets. *J Magn Magn Mater* 2018, **462**: 220–225.
[157] Sukthavorn K, Phengphon N, Nootsuwan N, *et al.* Effect of silane coupling on the properties of polylactic acid/barium ferrite magnetic composite filament for the 3D printing process. *J Appl Polym Sci* 2021, **138**: 50965.
[158] Schönrath H, Spasova M, Kilian SO, *et al.* Additive manufacturing of soft magnetic permalloy from Fe and Ni powders: Control of magnetic anisotropy. *J Magn Magn Mater* 2019, **478**: 274–278.
[159] Chaudhary V, Nartu MSKKY, Mantri SA, *et al.* Additive manufacturing of functionally graded Co–Fe and Ni–Fe magnetic materials. *J Alloys Compd* 2020, **823**: 153817.
[160] Garibaldi M, Ashcroft I, Lemke JN, *et al.* Effect of annealing on the microstructure and magnetic properties of soft magnetic Fe–Si produced via laser additive manufacturing. *Scripta Mater* 2018, **142**: 121–125.
[161] Yang XS, Cui XF, Jin G, *et al.* Soft magnetic property of $(Fe_{60}Co_{35}Ni_5)_{78}Si_6B_{12}Cu_1Mo_3$ alloys by laser additive manufacturing. *J Magn Magn Mater* 2018, **466**: 75–80.
[162] An T, Hwang KT, Kim JH, *et al.* Extrusion-based 3D direct ink writing of NiZn-ferrite structures with viscoelastic ceramic suspension. *Ceram Int* 2020, **46**: 6469–6476.
[163] Liu LB, Ngo KDT, Lu GQ. Guideline for paste extrusion 3D printing of slump-free ferrite inductor cores. *Ceram Int* 2021, **47**: 5803–5811.
[164] Liu LB, Ngo KDT, Lu GQ. Effects of Co_3O_4 addition on magnetic properties of NiCuZn ferrite feedstock for 3D-printing power magnetic components. *IEEE Trans Magn* 2020, **56**: 2000307.
[165] Liu LB, Ngo KDT, Lu GQ. Effects of SiO_2 inclusions on sintering and permeability of NiCuZn ferrite for additive manufacturing of power magnets. *J Eur Ceram Soc* 2021, **41**: 466–471.
[166] Ye FJ, Dai HY, Peng K, *et al.* Effect of Mn doping on the microstructure and magnetic properties of $CuFeO_2$ ceramics. *J Adv Ceram* 2020, **9**: 444–453.
[167] Phor L, Chahal S, Kumar V. Zn^{2+} substituted superparamagnetic $MgFe_2O_4$ spinel-ferrites: Investigations on structural and spin-interactions. *J Adv Ceram* 2020, **9**: 576–587.
[168] Aqzna SS, Yeoh CK, Idris MS, *et al.* Effect of different filler content of ABS–zinc ferrite composites on mechanical, electrical and thermal conductivity by using 3D printing. *J Vinyl Addit Technol* 2018, **24**: E217–E229.
[169] Wang YQ, Castles F, Grant PS. 3D printing of NiZn ferrite/ABS magnetic composites for electromagnetic devices. *MRS Proc* 2015, **1788**: 29–35.
[170] Bissannagari M, Kim TH, Yook JG, *et al.* All inkjet-printed flexible wireless power transfer module: PI/Ag hybrid spiral coil built into 3D NiZn-ferrite trench structure with a resonance capacitor. *Nano Energy* 2019, **62**: 645–652.
[171] Razzaq MY, Behl M, Kratz K, *et al.* Multifunctional hybrid nanocomposites with magnetically controlled reversible shape-memory effect. *Adv Mater* 2013, **25**: 5730–5733.
[172] Thévenot J, Oliveira H, Sandre O, *et al.* Magnetic responsive polymer composite materials. *Chem Soc Rev* 2013, **42**: 7099–7116.
[173] Li YY, Liu QK, Hess AJ, *et al.* Programmable ultralight magnets via orientational arrangement of ferromagnetic nanoparticles within aerogel hosts. *ACS Nano* 2019, **13**: 13875–13883.
[174] Cuchet C, Muster A, Germano P, *et al.* Soft magnets implementation using a stereolithography-based 3D printer. In: Proceedings of the 2017 20th International Conference on Electrical Machines and Systems, Sydney, Australia, 2017: 8056301.
[175] Palmero EM, Rial J, de Vicente J, *et al.* Development of permanent magnet MnAlC/polymer composites and flexible filament for bonding and 3D-printing technologies. *Sci Technol Adv Mater* 2018, **19**: 465–473.
[176] Khatri B, Lappe K, Noetzel D, *et al.* A 3D-printable polymer-metal soft-magnetic functional composite—Development and characterization. *Materials* 2018, **11**: 189.
[177] Guan XN, Xu XN, Kuniyoshi R, *et al.* Electromagnetic and mechanical properties of carbonyl iron powders-PLA

composites fabricated by fused deposition modeling. *Mater Res Express* 2018, **5**: 115303.
[178] Liu LB, Ge T, Ngo KDT, *et al.* Ferrite paste cured with ultraviolet light for additive manufacturing of magnetic components for power electronics. *IEEE Magn Lett* 2018, **9**: 5102705.
[179] Roh S, Okello LB, Golbasi N, *et al.* 3D-printed silicone soft architectures with programmed magneto-capillary reconfiguration. *Adv Mater Technol* 2019, **4**: 1800528.
[180] Kang BJ, Lee CK, Oh JH. All-inkjet-printed electrical components and circuit fabrication on a plastic substrate. *Microelectron Eng* 2012, **97**: 251–254.
[181] Credi C, Fiorese A, Tironi M, *et al.* 3D printing of cantilever-type microstructures by stereolithography of ferromagnetic photopolymers. *ACS Appl Mater Interfaces* 2016, **8**: 26332–26342.
[182] Löwa N, Fabert JM, Gutkelch D, *et al.* 3D-printing of novel magnetic composites based on magnetic nanoparticles and photopolymers. *J Magn Magn Mater* 2019, **469**: 456–460.
[183] Bastola AK, Hoang VT, Li L. A novel hybrid magnetorheological elastomer developed by 3D printing. *Mater Des* 2017, **114**: 391–397.
[184] Bastola AK, Paudel M, Li L. Development of hybrid magnetorheological elastomers by 3D printing. *Polymer* 2018, **149**: 213–228.
[185] Chen ZP, Ren L, Li JY, *et al.* Rapid fabrication of microneedles using magnetorheological drawing lithography. *Acta Biomater* 2018, **65**: 283–291.
[186] Sindersberger D, Diermeier A, Prem N, *et al.* Printing of hybrid magneto active polymers with 6 degrees of freedom. *Mater Today Commun* 2018, **15**: 269–274.
[187] Tiberto P, Barrera G, Celegato F, *et al.* Magnetic properties of jet-printer inks containing dispersed magnetite nanoparticles. *Eur Phys J B* 2013, **86**: 173.
[188] Saleh E, Woolliams P, Clarke B, *et al.* 3D inkjet-printed UV-curable inks for multi-functional electromagnetic applications. *Addit Manuf* 2017, **13**: 143–148.
[189] Kim J, Chung SE, Choi SE, *et al.* Programming magnetic anisotropy in polymeric microactuators. *Nat Mater* 2011, **10**: 747–752.
[190] Erb RM, Martin JJ, Soheilian R, *et al.* Actuating soft matter with magnetic torque. *Adv Funct Mater* 2016, **26**: 3859–3880.
[191] Truby RL, Lewis JA. Printing soft matter in three dimensions. *Nature* 2016, **540**: 371–378.
[192] Ionov L. Biomimetic hydrogel-based actuating systems. *Adv Funct Mater* 2013, **23**: 4555–4570.
[193] Tabatabaei SN, Lapointe J, Martel S. Shrinkable hydrogel-based magnetic microrobots for interventions in the vascular network. *Adv Robotics* 2011, **25**: 1049–1067.
[194] Suzumori K. Elastic materials producing compliant robots. *Robotics Auton Syst* 1996, **18**: 135–140.
[195] Rus D, Tolley MT. Design, fabrication and control of soft robots. *Nature* 2015, **521**: 467–475.
[196] Kim SW, Lee SM, Lee JH, *et al.* Fabrication and manipulation of ciliary microrobots with non-reciprocal magnetic actuation. *Sci Rep* 2016, **6**: 30713.
[197] Diller E, Sitti M. Three-dimensional programmable assembly by untethered magnetic robotic micro-grippers. *Adv Funct Mater* 2014, **24**: 4397–4404.
[198] Hu W, Lum GZ, Mastrangeli M, *et al.* Small-scale soft-bodied robot with multimodal locomotion. *Nature* 2018, **554**: 81–85.
[199] Wehner M, Truby RL, Fitzgerald DJ, *et al.* An integrated design and fabrication strategy for entirely soft, autonomous robots. *Nature* 2016, **536**: 451–455.
[200] Joyee EB, Pan YY. A fully three-dimensional printed inchworm-inspired soft robot with magnetic actuation. *Soft Robotics* 2019, **6**: 333–345.
[201] Keneth ES, Epstein AR, Harari MS, *et al.* 3D printed ferrofluid based soft actuators. In: Proceedings of the 2019 International Conference on Robotics and Automation, Montreal, Canada, 2019: 7569–7574.
[202] de Marco C, Alcântara CCJ, Kim S, *et al.* Indirect 3D and 4D printing of soft robotic microstructures. *Adv Mater Technol* 2019, **4**: 1900332.
[203] Zhao XH, Kim YH. Soft microbots programmed by nanomagnets. *Nature* 2019, **575**: 58–59.
[204] Chen XZ, Hoop M, Mushtaq F, *et al.* Recent developments in magnetically driven micro- and nanorobots. *Appl Mater Today* 2017, **9**: 37–48.
[205] Peters C, Hoop M, Pané S, *et al.* Degradable magnetic composites for minimally invasive interventions: Device fabrication, targeted drug delivery, and cytotoxicity tests. *Adv Mater* 2016, **28**: 533–538.
[206] Kim Y, Parada GA, Liu SD, *et al.* Ferromagnetic soft continuum robots. *Sci Robot* 2019, **4**: eaax7329.
[207] Macdonald E, Salas R, Espalin D, *et al.* 3D printing for the rapid prototyping of structural electronics. *IEEE Access* 2014, **2**: 234–242.
[208] Liang W, Raymond L, Rivas J. 3D printed air core inductors for high frequency power converters. *IEEE Trans Power Electron* 2016, **31**: 52–64.
[209] Huang SH, Liu P, Mokasdar A, *et al.* Additive manufacturing and its societal impact: A literature review. *Int J Adv Manuf Technol* 2013, **67**: 1191–1203.
[210] Yan Y, Moss J, Ngo KDT, *et al.* Additive manufacturing of toroid inductor for power electronics applications. *IEEE Trans Ind Appl* 2017, **53**: 5709–5714.
[211] Lazarus N, Bedair SS, Smith GL. Creating 3D printed magnetic devices with ferrofluids and liquid metals. *Addit Manuf* 2019, **26**: 15–21.
[212] Sochol RD, Sweet E, Glick CC, *et al.* 3D printed microfluidics and microelectronics. *Microelectron Eng* 2018, **189**: 52–68.
[213] Yuan S, Huang Y, Zhou JF, *et al.* Magnetic field energy harvesting under overhead power lines. *IEEE Trans Power Electron* 2015, **30**: 6191–6202.
[214] Han JC, Hu J, Wang SX, *et al.* Magnetic energy harvesting properties of piezofiber bimorph/NdFeB composites. *Appl Phys Lett* 2014, **104**: 093901.

[215] Qiu J, Wen YM, Li P, *et al.* Design and testing of piezoelectric energy harvester for powering wireless sensors of electric line monitoring system. *J Appl Phys* 2012, **111**: 07E510.
[216] Wang ZX, Hu J, Han JC, *et al.* A novel high-performance energy harvester based on nonlinear resonance for scavenging power-frequency magnetic energy. *IEEE Trans Ind Electron* 2017, **64**: 6556–6564.
[217] Wang ZX, Huber C, Hu J, *et al.* An electrodynamic energy harvester with a 3D printed magnet and optimized topology. *Appl Phys Lett* 2019, **114**: 013902.
[218] Urbanek S, Ponick B, Taube A, *et al.* Additive manufacturing of a soft magnetic rotor active part and shaft for a permanent magnet synchronous machine. In: Proceedings of the 2018 IEEE Transportation Electrification Conference and Expo, Long Beach, USA, 2018: 668–674.
[219] Liaw CY, Guvendiren M. Current and emerging applications of 3D printing in medicine. *Biofabrication* 2017, **9**: 024102.
[220] Zhang YL, Yang B, Zhang XY, *et al.* A magnetic self-healing hydrogel. *Chem Commun* 2012, **48**: 9305–9307.
[221] Bhattacharya S, Eckert F, Boyko V, *et al.* Temperature-, pH-, and magnetic-field-sensitive hybrid microgels. *Small* 2007, **3**: 650–657.
[222] Chen XZ, Hoop M, Shamsudhin N, *et al.* Hybrid magnetoelectric nanowires for nanorobotic applications: Fabrication, magnetoelectric coupling, and magnetically assisted *in vitro* targeted drug delivery. *Adv Mater* 2017, **29**: 1605458.
[223] Chin SY, Poh YC, Kohler AC, *et al.* Additive manufacturing of hydrogel-based materials for next-generation implantable medical devices. *Sci Robot* 2017, **2**: eaah6451.
[224] Lin HY, Huang HY, Shiue SJ, *et al.* Osteogenic effects of inductive coupling magnetism from magnetic 3D printed hydrogel scaffold. *J Magn Magn Mater* 2020, **504**: 166680.
[225] Li XJ, Shan WT, Yang Y, *et al.* Painless microneedles: Limpet tooth-inspired painless microneedles fabricated by magnetic field-assisted 3D printing. *Adv Funct Mater* 2021, **31**: 2170033.
[226] Wu CT, Luo YX, Cuniberti G, *et al.* Three-dimensional printing of hierarchical and tough mesoporous bioactive glass scaffolds with a controllable pore architecture, excellent mechanical strength and mineralization ability. *Acta Biomater* 2011, **7**: 2644–2650.
[227] Luo YX, Wu CT, Lode A, *et al.* Hierarchical mesoporous bioactive glass/alginate composite scaffolds fabricated by three-dimensional plotting for bone tissue engineering. *Biofabrication* 2013, **5**: 015005.
[228] Chen Z, Zhang DW, Peng E, *et al.* 3D-printed ceramic structures with *in situ* grown whiskers for effective oil/water separation. *Chem Eng J* 2019, **373**: 1223–1232.
[229] Zhong LS, Hu JS, Liang HP, *et al.* Self-assembled 3D flowerlike iron oxide nanostructures and their application in water treatment. *Adv Mater* 2006, **18**: 2426–2431.
[230] Yantasee W, Warner CL, Sangvanich T, *et al.* Removal of heavy metals from aqueous systems with thiol functionalized superparamagnetic nanoparticles. *Environ Sci Technol* 2007, **41**: 5114–5119.
[231] Chen K, He JY, Li YL, *et al.* Removal of cadmium and lead ions from water by sulfonated magnetic nanoparticle adsorbents. *J Colloid Interface Sci* 2017, **494**: 307–316.
[232] Meidanchi A, Akhavan O. Superparamagnetic zinc ferrite spinel–graphene nanostructures for fast wastewater purification. *Carbon* 2014, **69**: 230–238.
[233] Chandra V, Park J, Chun Y, *et al.* Water-dispersible magnetite-reduced graphene oxide composites for arsenic removal. *ACS Nano* 2010, **4**: 3979–3986.
[234] Hu JS, Zhong LS, Song WG, *et al.* Synthesis of hierarchically structured metal oxides and their application in heavy metal ion removal. *Adv Mater* 2008, **20**: 2977–2982.
[235] Kilianová M, Prucek R, Filip J, *et al.* Remarkable efficiency of ultrafine superparamagnetic iron(III) oxide nanoparticles toward arsenate removal from aqueous environment. *Chemosphere* 2013, **93**: 2690–2697.
[236] Huang SH, Chen DH. Rapid removal of heavy metal cations and anions from aqueous solutions by an amino-functionalized magnetic nano-adsorbent. *J Hazard Mater* 2009, **163**: 174–179.
[237] Yu XL, Tong SR, Ge MF, *et al.* One-step synthesis of magnetic composites of cellulose@iron oxide nanoparticles for arsenic removal. *J Mater Chem A* 2013, **1**: 959–965.
[238] Wang J, Zhang WT, Yue XY, *et al.* One-pot synthesis of multifunctional magnetic ferrite–MoS_2–carbon dot nanohybrid adsorbent for efficient Pb(II) removal. *J Mater Chem A* 2016, **4**: 3893–3900.
[239] Fu YS, Wang X. Magnetically separable $ZnFe_2O_4$–graphene catalyst and its high photocatalytic performance under visible light irradiation. *Ind Eng Chem Res* 2011, **50**: 7210–7218.
[240] Afkhami A, Sayari S, Moosavi R, *et al.* Magnetic nickel zinc ferrite nanocomposite as an efficient adsorbent for the removal of organic dyes from aqueous solutions. *J Ind Eng Chem* 2015, **21**: 920–924.
[241] Rajput S, Pittman Jr CU, Mohan D. Magnetic magnetite (Fe_3O_4) nanoparticle synthesis and applications for lead (Pb^{2+}) and chromium (Cr^{6+}) removal from water. *J Colloid Interface Sci* 2016, **468**: 334–346.
[242] Kumar S, Nair RR, Pillai PB, *et al.* Graphene oxide–$MnFe_2O_4$ magnetic nanohybrids for efficient removal of lead and arsenic from water. *ACS Appl Mater Interfaces* 2014, **6**: 17426–17436.
[243] Wu ZX, Li W, Webley PA, *et al.* General and controllable synthesis of novel mesoporous magnetic iron oxide@carbon encapsulates for efficient arsenic removal. *Adv Mater* 2012, **24**: 485–491.
[244] Venkateswarlu S, Yoon M. Core–shell ferromagnetic nanorod based on amine polymer composite (Fe_3O_4@DAPF) for fast removal of Pb(II) from aqueous solutions. *ACS Appl Mater Interfaces* 2015, **7**: 25362–25372.
[245] Sharma RK, Puri A, Monga Y, *et al.* Acetoacetanilide-functionalized Fe_3O_4 nanoparticles for selective and cyclic removal of Pb^{2+} ions from different charged wastewaters. *J*

Mater Chem A 2014, **2**: 12888–12898.

[246] Shen YF, Tang J, Nie ZH, *et al.* Preparation and application of magnetic Fe_3O_4 nanoparticles for wastewater purification. *Sep Purif Technol* 2009, **68**: 312–319.

[247] Dave PN, Chopda LV. Application of iron oxide nanomaterials for the removal of heavy metals. *J Nanotechnol* 2014, **2014**: 398569.

[248] Mou FZ, Pan D, Chen CR, *et al.* Magnetically modulated pot-like $MnFe_2O_4$ micromotors: Nanoparticle assembly fabrication and their capability for direct oil removal. *Adv Funct Mater* 2015, **25**: 6173–6181.

[249] Ambashta RD, Sillanpää M. Water purification using magnetic assistance: A review. *J Hazard Mater* 2010, **180**: 38–49.

[250] Gu SG, Lian F, Yan KJ, *et al.* Application of polymeric ferric sulfate combined with cross-frequency magnetic field in the printing and dyeing wastewater treatment. *Water Sci Technol* 2019, **80**: 1562–1570.

[251] Kim YG, Song JB, Yang DG, *et al.* Effects of filter shapes on the capture efficiency of a superconducting high-gradient magnetic separation system. *Supercond Sci Technol* 2013, **26**: 085002.

[252] Ditsch A, Lindenmann S, Laibinis PE, *et al.* High-gradient magnetic separation of magnetic nanoclusters. *Ind Eng Chem Res* 2005, **44**: 6824–6836.

[253] Wang FW, Tang DD, Gao LK, *et al.* Dynamic capture and accumulation of multiple types of magnetic particles based on fully coupled multiphysics model in multiwire matrix for high-gradient magnetic separation. *Adv Powder Technol* 2020, **31**: 1040–1050.

[254] Xue ZX, Wang YH, Zheng XY, *et al.* Particle capture of special cross-section matrices in axial high gradient magnet ic separation: A 3D simulation. *Sep Purif Technol* 2020, **237**: 116375.

[255] Hoffmann C, Franzreb M, Holl WH. A novel high-gradient magnetic separator (HGMS) design for biotech applications. *IEEE Trans Appl Supercond* 2002, **12**: 963–966.

[256] Svoboda J. A realistic description of the process of high-gradient magnetic separation. *Miner Eng* 2001, **14**: 1493–1503.

[257] Yavuz CT, Mayo JT, Yu WW, *et al.* Low-field magnetic separation of monodisperse Fe_3O_4 nanocrystals. *Science* 2006, **314**: 964–967.

[258] Gheisari K, Shahriari S, Javadpour S. Structure and magnetic properties of ball-mill prepared nanocrystalline Ni–Zn ferrite powders at elevated temperatures. *J Alloys Compd* 2013, **552**: 146–151.

[259] Sharma R, Singhal S. Structural, magnetic and electrical properties of zinc doped nickel ferrite and their application in photo catalytic degradation of methylene blue. *Phys B Condens Matter* 2013, **414**: 83–90.

[260] Raghavender AT, Hoa Hong N, Chikoidze E, *et al.* Effect of zinc doping on the structural and magnetic properties of nickel ferrite thin films fabricated by pulsed laser deposition technique. *J Magn Magn Mater* 2015, **378**: 358–361.

[261] Zhu WM, Wang L, Zhao R, *et al.* Electromagnetic and microwave-absorbing properties of magnetic nickel ferrite nanocrystals. *Nanoscale* 2011, **3**: 2862–2864.

[262] Tang SCN, Yan DYS, Lo IMC. Sustainable wastewater treatment using microsized magnetic hydrogel with magnetic separation technology. *Ind Eng Chem Res* 2014, **53**: 15718–15724.

[263] Chowdhury MR, Steffes J, Huey BD, *et al.* 3D printed polyamide membranes for desalination. *Science* 2018, **361**: 682–686.

[264] Peyer KE, Zhang L, Nelson BJ. Bio-inspired magnetic swimming microrobots for biomedical applications. *Nanoscale* 2013, **5**: 1259–1272.

[265] Nelson BJ, Kaliakatsos IK, Abbott JJ. Microrobots for minimally invasive medicine. *Annu Rev Biomed Eng* 2010, **12**: 55–85.

[266] Klumpp S, Lefèvre CT, Bennet M, *et al.* Swimming with magnets: From biological organisms to synthetic devices. *Phys Rep* 2019, **789**: 1–54.

[267] Hsu A, Chu W, Cowan C, *et al.* Diamagnetically levitated milli-robots for heterogeneous 3D assembly. *J Micro Bio Robotics* 2018, **14**: 1–16.

[268] Ghosh D, Gupta T, Sahu RP, *et al.* Three-dimensional printing of diamagnetic microparticles in paramagnetic and diamagnetic media. *Phys Fluids* 2020, **32**: 072001.

[269] Lei L, Liu L, Wang XT, *et al.* Strongly improved current-carrying capacity induced by nanoscale lattice strains in $YBa_2Cu_3O_{7-\delta}$–$Ba_{0.7}Sr_{0.3}TiO_3$ composite films derived from chemical solution deposition. *J Mater Chem C* 2016, **4**: 1392–1397.

[270] Albiss BA, Obaidat IM. Applications of YBCO-coated conductors: A focus on the chemical solution deposition method. *J Mater Chem* 2010, **20**: 1836–1845.

[271] Tiismus H, Kallaste A, Belahcen A, *et al.* Hysteresis measurements and numerical losses segregation of additively manufactured silicon steel for 3D printing electrical machines. *Appl Sci* 2020, **10**: 6515.